SOLAR AXION SEARCH WITH THE CAST EXPERIMENT

NATIONAL **T**ECHNICAL **U**NIVERSITY OF **A**THENS
School of Applied Mathematical and Physical Sciences
Department of Physics
Group of Experimental High Energy Physics

DIPLOMA THESIS

Theofani D. Karageorgopoulou

Supervisor: Evangelos N. Gazis
Professor, NTUA

Σε αυτούς που πίστεψαν,
άνευ όρων.

Στην οικογένεια που έχουμε,
τόσο εκ γενετής όσο και από επιλογή.

Στους γονείς μου και τον αδερφό μου.

Ένα βήμα κάθε φορά…

Περίληψη

Η συμμετρία φορτίου-ομοτιμίας (CP Symmetry) αποτελεί τη σύζευξη των συμμετριών φορτίου (C Symmetry) και ομοτιμίας (P Symmetry) και θεωρητικά προβλέπεται η παραβίασή της έτσι ώστε να εξηγείται η υπερίσχυση της ύλης έναντι της αντιύλης στις στιγμές που ακολούθησαν τη Μεγάλη Έκρηξη. Η παραβίασή της από τις ασθενείς αλληλεπιδράσεις αποδείχθηκε πειραματικά το 1964 από τους James W. Cronin και Val L. Fitch. Ωστόσο, η Κβαντική Χρωμοδυναμική (QCD), η οποία αποτελεί την επικρατέστερη θεωρία περιγραφής των ισχυρών αλληλεπιδράσεων μεταξύ των quarks και των γκλουονίων, δε φαίνεται να την παραβιάζει κάτι που αντιτίθεται στη θεωρητική πρόβλεψη.

Πράγματι, μη διαταρακτικά φαινόμενα της Κβαντικής Χρωμοδυναμικής μπορούν να επάγουν έναν επιπλέον όρο στη λαγκρανζιανή του Καθιερωμένου Προτύπου ο οποίος οδηγεί στην παραβίαση της συμετρίας φορτίου-ομοτιμίας. Ωστόσο, καμμία πειραματική ένδειξη για κάτι τέτοιο δεν υπάρχει μέχρι σήμερα. Αυτή η συμπεριφορά της Κβαντικής Χρωμοδυναμικής συνιστά ένα πρόβλημα γνωστό σαν «Ισχυρό Πρόβλημα CP» ή «Πρόθλημα θ» (Strong CP Problem) το οποίο δεν είναι δυνατό να λυθεί στα πλαίσια του Καθιερωμένου Προτύπου.

Οι πιθανές λύσεις του προβλήματος θ είναι τρεις και είναι οι εξής:

1. Πιθανή απαλοιφή της μάζας του up quark.
2. Πιθανή αυθόρμητη παραβίαση της συμμετρίας CP σύμφωνα με το μηχανισμό Nelson-Barr.
3. Ύπαρξη ενός υποθετικού σωματιδίου, του αξιονίου, όπως προβλέπεται θεωρητικά από τον μηχανισμό Peccei-Quinn (PQ Mechanism).

Η επικρατέστερη των λύσεων είναι αυτή που προτάθηκε από τους R. Peccei και H. Quinn το 1977, σύμφωνα με την οποία εισάγεται μια νέα συμμετρία, η $U(1)_{PQ}$, η οποία παραβιάζεται αυθόρμητα σε κάποια ενεργειακή κλίμακα οδηγώντας σε ένα καινούριο σωματίδιο, το αξιόνιο. Το σωματίδιο αυτό θα πρέπει να έχει πάρα πολύ μικρή μάζα, ουδέτερο ηλεκτρικό φορτίο καθώς και πολύ μικρή σταθερά σύζευξης με τα λεπτόνια και τα quarks, δηλαδή πολύ μικρές ενεργές διατομές στην περίπτωση των ασθενών και των ισχυρών αλληλεπιδράσεων αντίστοιχα.

Πέραν της επίλυσης του Ισχυρού Προβλήματος CP της Κβαντικής Χρωμοδυναμικής, τα αξιόνια, αν τελικά υπάρχουν, έχουν και κοσμολογικές προεκτάσεις αφού πιθανότατα αποτελούν τμήμα μέρους της σκοτεινής ύλης για μάζες γύρω στα 1-2 GeV η οποία είναι γνωστή ως «ψυχρή σκοτεινή ύλη». Έταιροι υποψήφιοι για αυτή τη θέση είναι τα διάφορα ασθενώς αλληλεπιδρώντα σωματίδια (Weakly Interacting Massive Particles – WIMPs).

Τα αξιόνια με ηλιακή προέλευση εικάζεται θεωρητικά ότι παράγονται μέσω του φαινομένου Primakoff, δηλαδή ως αποτέλεσμα της διέλευσης φωτονίων μέσω δυνατού μαγνητικού πεδίου. Αυτή τους η ιδιότητα είναι που χρησιμοποιείται και ως αρχή ανίχνευσής τους στο πείραμα CAST (CERN Axion Solar Telescope) του Ευρωπαϊκού Κέντρου Πυρηνικών Ερευνών (CERN). Στο πείραμα CAST, ακτινοβολία προερχόμενη από τον Ήλιο διέρχεται από ισχυρό

μαγνητικό πεδίο που δημιουργείται με τη βοήθεια μαγνήτη ο οποίος έχει κατασκευαστεί για τον Μεγάλο Αδρονικό Επιταχυντή (LHC). Έτσι, τα αξιόνια που πιθανόν συμπεριλαμβάνονται στην ακτινοβολία υπόκεινται στο αντίστροφο του μηχανισμού Primakoff με απώτερο σκοπό την μετατροπή τους σε φωτόνια και την ανίχνευσή τους από τα κατάλληλα ανιχνευτικά συστήματα.

Η 1η Φάση του πειράματος CAST έλαβε χώρα από το 2003 εώς και το 2004. Καθόλη τη διάρκεια αυτής της Φάσης, το πείραμα διεξήχθηκε με κενό στο εσωτερικό των σωλήνων του μαγνήτη. Δεν ανιχνεύθηκε κανένα σήμα αξιονίου, γεγονός που είχε σαν αποτέλεσμα νέα οριακή τιμή για τη σταθερά σύζευξης αξιονίου με φωτόνιο: $g_{a\gamma} < 1.16 \cdot 10^{-10} GeV^{-1}$. Η 2η Φάση του πειράματος χαρακτηρίζεται από την πλήρωση των σωλήνων του μαγνήτη με ^{4}He για την περίοδο 2005-2006 και με ^{3}He για την περίοδο 2008 μέχρι και σήμερα. Η περίοδος του ^{4}He επίσης δε σηματοδοτήθηκε από κάποια ανακάλυψη, ωστόσο υπήρξε εκ νέου βελτίωση του άνω ορίου της σταθεράς σύζευξης του αξιονίου με το φωτόνιο: $g_{a\gamma} < 8.8 \cdot 10^{-11} GeV^{-1}$.

Σκοπός της συγκεκριμένης εργασίας είναι η εκτενής ανάλυση των φαινομένων και της θεωρίας στην οποία στηρίζεται η ύπαρξη των αξιονίων καθώς και η περιγραφή του πειράματος CAST. Η συγγραφή της εργασίας αυτής βασίζεται στην ενασχόλησή μου ως μέλος του πειράματος CAST στα διάφορα στάδια της προετοιμασίας της 2ης Φάσης του πειράματος για τη λειτουργία με ^{3}He καθώς και της λειτουργίας του καθεαυτής από τον Αύγουστο 2007 μέχρι και τον Αύγουστο του 2009.

To the ones who believed,
no matter what.

To the family we have,
by birth and choice too.

To my parents and my brother.

One step at a time…

Abstract

CP Symmetry is a result of the conjugation of both Charge and Parity Symmetries and is theoretically expected to be violated in order to be able to explain why matter has succeeded to dominate over antimatter after the Big Bang occurred. It's violation under weak interactions was experimentally proven in 1964 by James W. Cronin and Val L. Fitch. However, Quantum Chromodynamics (QCD), which is the strongest theory describing the strong interactions between quarks and gluons, doesn't seem to violate it, a fact that opposes theoretical predictions.

Non-perturbative effects of QCD are indeed able to postulate an additional factor into the Standard Model lagrangian, a factor that leads into the violation of CP Symmetry. However, no such experimental evidence has ever been observed. This behaviour of QCD leads to a problem known as "Strong CP Problem" which can't be solved in terms of the Standard Model.

The possible solutions of the Strong CP Problem are the following three:

1. Possible vanishing of the up quark mass.
2. Possible spontaneous violation of the CP Symmetry through the Nelson-Barr Mechanism
3. Existence of a hypothetical particle, the axion, as it is theoretically expected to be created through the Peccei-Quinn Mechanism.

The most elegant of the solutions and the one believed to be the real case is the one proposed by R. Peccei and H. Quinn in 1977. According to them, a new $U(1)_{PQ}$ symmetry is being introduced and as it is spontaneously violated in some energy scale a new particle occures, the axion. This particle has to have a very small mass, no electric charge and really small cross sections when it comes to weak and strong interactions.

Except for providing a solution to the Strong CP Problem of QCD, axions, if they are finally proven to exist, are candidates for a piece of the Dark Matter pie. Their co-candidates are the various Weakly Interacting Massive Particles (WIMPs).

Solar Axions are believed to be produced through the Primakoff process where photons traveling through a strong magnetic field are converted into particles. This property of theirs is which is used as detection principle at the CAST Experiment (CERN Axion Solar Telescope) at the European Organisation for Nuclear Research (CERN). At the CAST Experiment, radiation deriving from the Sun enters a strong magnetic field produced by one of the magnets constructed for the LHC. There, if any axion is present it subjects to the reverse Primakoff mechanism and is being converted to a photon of characterstic energy so it can be detected by the appropriate detecting devices.

CAST Phase I was held through 2003 and 2004. During Phase I, the experiment run under vacuum conditions in both magnet's bores. No signal above background was observed and so the upper limit for the axion photon coupling was calculated to be $g_{a\gamma} < 1.16 \cdot 10^{-10} GeV^{-1}$. CAST Phase II differentiated

the experiment by having the bores filled firstly with ^{4}He (2005-2006) and then with ^{3}He (2008-now). ^{4}He era was also signal-free but re-evaluated the upper limit for the axion photon coupling to $g_{a\gamma} < 8.8 \cdot 10^{-11} GeV^{-1}$.

This thesis aims to extensively analyze the axion motivation theory and also describe in detail the CAST Experiment. The writing of this thesis is a result of myself being occupied as a member of the CAST Experiment in the various stages of the preparation of the Phase II-^{3}He runs and it's function in general for the period August 2007 – August 2010.

Contents

Chapter 1

AXION MOTIVATION

INTRODUCTION

Quantum Chromodynamics is the theory describing the strong interactions among quarks and gluons. It is theoretically expected to violate the CP Symmetry as being done by weak interactions. However, this behavior has never been exhibited by nature, experimental fact that constitutes the so-called “Strong CP Problem”.

There are three proposed solutions to the Strong CP Problem with the most common being the existence of a new scalar particle, the axion. This solution was proposed by R. Peccei and H. Quinn in 1977 and is considered to be the most elegant of all.

In this Chapter, the theoretical ground of axion’s motivation is being set and well described.

1.1 Introduction to Symmetries

1.1.1 C Symmetry

In elementary particle physics, the term "C Symmetry" refers to the symmetry of physical laws under a charge conjugation transformation which is the operation that converts each particle into its antiparticle. It is an extension of the ivariance of classical electrodynamics in every sign change of electric charges.

C Symmetry is obeyed by electromagnetism, gravity and strong interactions. However, when it comes to weak interactions someone can notice that when C Symmetry is applied to a neutrino, which is a priori left-handed, a left-handed antineutrino is expected, something that doesn't exist. Hence, weak interactions are C violating.

In electromagnetism, more extensively, every charge q is replaced by a charge –q and the directions of the electric and magnetic fields are reversed so that the dynamics behind the electromagnetic laws are preserved. When applying the C Symmetry, we face the following transformations:

$$\psi \rightarrow -i(\overline{\psi}\gamma^0\gamma^2)^T$$
$$\overline{\psi} \rightarrow -i(\gamma^0\gamma^2\psi)^T$$
$$A^\mu \rightarrow -A^\mu$$

The transformations above do not affect the chiralty of the particles concluding to a left-handed antineutrino when C Symmetry is applied on a left-handed neutrino, which, of course, is impossible.

1.1.2 P Symmetry

In elementary particle physics, parity transformation is a result of the corresponding operator P acting on a system causing the simulatneous flip in the sign of all spatial coordinates:

$$P:\begin{pmatrix} x \\ y \\ z \end{pmatrix} \rightarrow \begin{pmatrix} -x \\ -y \\ -z \end{pmatrix}$$
$$P\psi(\vec{r}) \rightarrow \psi(-\vec{r})$$

It is more than obvious that if we apply the parity operator P on a system two times consecutively, we will finally reach its initial state, meaning $P^2=1$. Consequently, P is a unitary operator and its only possible eigenvalues (if existing) are P=+1 and P=-1. This is why a wavefunction ψ can only have a well-defined parity, which will be either even (P=+1) or odd (P=-1).

Schematically, we may consider parity as the inversion of an observed state through the origin of the coordinate system to the diametrically opposite location. The corresponding mathematical notion is that of a point reflection and a consecutive rotation. The previous fact results naturally if we consider that a 3×3 matrix representation of parity and it's corresponding operator P would

lead to a determinant equal to -1 and consequently could not reduce to a mere rotation which requires a determinant equal to 1. Furthermore, it is accepted that this transformation does not affect all the other internal properties of a particle like it's electric charge or it's baryonic/leptonic number etc. when these properties are invariant of the natural spacetime.

Parity is conserved when the corresponding operator P commutes with the Hamiltonian H of the system, meaning [H,P]=0. When P is applied to a system, it doesn't change it's spin but it does change its momentum so that the helicity of the particle is affected too changing a left-handed particle to a right-handed one.

Experimental facts show that strong and electromagnetic interactions are invariant under parity transformations but only when the internal parity of the particles is taken into account, making laws of both theories ambidextrous. The internal parity of every particle is characteristic for every particle and is invariant of its movement state. Contrasting to the strong and electromagnetic interactions, weak interactions do not conserve parity[1] meaning that every interaction happening due to weak interactions doesn't occur similarly in inversed space. This behaviour is exhibited due to the so-called maximum parity violation principle, which implies that in V-A Theory (the universal theory describing the weak interactions) where the matrix elements include superpositions of amplitudes with even and odd parities where these amplitudes are almost equal, making parity violation the signature of weak interactions.

However, even in strong and electromagnetic interactions there has been experimentally shown that in a small percentage P Symmetry is violated. This violation doesn't result from P Symmetry collapsing in terms of those theories but from the fact that the Hamiltonian describing every interaction inevitably includes contributions from weak interactions among the particles involved:

$$H = H_{strong} + H_{electromagnetic} + H_{weak}$$

In spite of its violation in weak processes, P Symmetry remains a valid symmetry of strong and electromagnetic processes, hence certain formalism and terminology have been developed. First of all, we have to establish a distinction among the geometrical entities. This distinction is shown in terms of the eigenvalues of the P operator in every case:

Geometrical Entity	**P**
Scalar	+1
Pseudoscalar	-1
Vector (Polar Vector)	-1
Pseudovector (Axial Vector)	+1

[1] The violation of parity in weak interactions was for the first time argued by Tsung Dao Lee and Chen Ning Yang, a proposal experimentally established by Chien-Shiung Wu through studying beta-transition of polarized Cobalt nuclei and finally awarded with the Nobel Prize of 1957. However, re-evaluation of experimental data of 1928 showed that parity violation had already been exhibited but those results were of no impact due to the experimental beliefs of this period of time.

As previously mentioned, when applied twice, the P operator drives every system back to its initial state:

$$P^2 = I$$

Hence, parity forms the Abelian group Z_2 with two irreducible representations, the first being even under parity and the latter odd.

1.1.3 CP Symmetry

Weak interactions are C and P Symmetry violating as shown in the preceding sections. The effort of skipping these two violations resulted to a new symmetry, which is the combination of these two symmetries. CP Symmetry was originally proposed in the 1950s[2], after the discovery of parity violation, a discovery with tremendous impact to the scientific community. Parity violation initialized studies on Hilbert space and its structure, which concluded to admitting that the symmetry of a quantum mechanical system can be restored if another symmetry can be found so the new combined symmetry remains unbroken. The symmetry that would restore order was proposed to be charge conjugation.

CP Symmetry is the product of the two problematic –when referring to weak interactions- symmetries: C and P. CP Symmetry says that the laws of physics should not change when the charge is flipped and the mirror image of the system is taken. This symmetry restored order into the Standard Model, though only for a short while since its violation was to be discovered in the near future.

CP Symmetry is obeyed by both strong and electromagnetic interactions. However, weak interactions are slightly violating it[3]. The most outstanding evidence of the CP Symmetry violation is the observed asymmetry of matter and antimatter in the Universe. Experimental data shows that approximately 34% of K_L^o[4] decays are of the 3π mode. However, there is a 41% that decays either to $\pi^+ + e^- + \bar{\nu}_e$ or to $\pi^- + e^+ + \nu_e$. One would expect those two decay modes to appear equally often. On the contrary, nature treats those two modes unequally by showing preference to create positrons stating the first experimental proof of an absolute distinction between matter and antimatter. Thus, it is firmly believed that CP violation may be responsible for the dominance of matter over antimatter.

In the Standard Model, CP violation's roots can be found using the Cabbibo-Kobayashi-Maskawa matrix (CKM). The CKM matrix, also know as quark-mixing matrix, is a 3× 3 unitary matrix defined for six quarks describing the probability of a transition from one quark to another through weak interactions. This matrix, which is an extension of Cabbibo's 2× 2 initial matrix

---

[2] In 1957, L. Davidovic Landau proposed CP symmetry as the true symmetry between matter and antimatter.

[3] CP Symmetry violation has been observed in weak interactions involving Kaons and B mesons. CP violation in K^0 decays was discovered in 1964 by James W. Cronin and Val L. Fitch, a discovery awarded with the Nobel Prize of 1980.

[4] K^0 decays with two different lifetimes: $\tau(K_S^o)=0.9\cdot 10^{-10}$ sec and $\tau(K_L^o)=0.5\cdot 10^{-7}$ sec. The beam used in the Cronin-Fitch experiment consisted of K_L^o particles.

and the Glashow-Iliopoulos-Maiani mechanism (GIM mechanism), includes all three generation of quarks.[5] The presence of three generations is the necessary condition for the existence of the complex phase in the CKM matrix that evokes CP violation. When combined to a vector of mass eigenstates of down-type quarks, CKM results to the weak interaction doublet partners of up-type quarks:

$$\begin{pmatrix} V_{ud} & V_{us} & V_{ub} \\ V_{cd} & V_{cs} & V_{cb} \\ V_{td} & V_{ts} & V_{tb} \end{pmatrix} \begin{pmatrix} |d\rangle \\ |s\rangle \\ |b\rangle \end{pmatrix} = \begin{pmatrix} |d'\rangle \\ |s'\rangle \\ |b'\rangle \end{pmatrix}$$

As previously mentioned, the CKM matrix describes the probability of a transition from one quark i to another quark j. These transitions are proportional to $|V_{ij}|^2$. In order to reach to an interesting result, the number of the parameters in this matrix has to be counted. If there are ν generations of quarks, then there are 2ν flavors. In a ν×ν matrix, there are ν^2 real parameters to be specified, 2ν-1 of them are not of physical importance resulting to $(\nu-1)^2$ free variables independent of the choice of the phases of basis vectors. Of these, $\nu(\nu-1)/2$ are rotation angles called quark mixing angles and the remaining $(\nu-1)(\nu-2)/2$ are the complex phases causing CP violation. In the Standard Model where three generations of quarks are known we obviously have one CP-violating complex phase.

In 1964, James W. Cronin and Val L. Fitch provided clear evidence that CP Symmetry can also be broken[6]. Through their work, in which they studied the decay of neutral Kaons, it was shown that weak interactions not only violate C and P Symmetries, but also their combination. This discovery arose questions of cosmological interest but also lead to the creation of a new symmetry, CPT, which also includes a third operator T referring to time reversal and corresponding to reversal of motion. CPT Symmetry is still believed to be an exact symmetry of all fundamental interactions.

However, CP violation has not been exhibited only in the sector of K-mesons, as it was firstly believed. In 2001, several experiments including the BaBar (Stanford Linear Accelerator Center-SLAC/USA) and the Belle Experiment (High Energy Accelerator Research Organization-KEK/Japan) observed direct CP violation in decays of the B-mesons.

CP violation is of a great importance in terms of Cosmology because it explains successfully the dominance of matter over antimatter in the Universe. It is an indisputable fact that the Universe is made mostly of matter, rather than consisting of equal parts of matter and antimatter. In order to create such an imbalance between matter and antimatter, the Sakharov conditions must be

[5] It should be pointed out that the CKM matrix proposed a third quark generation when even the second one was not yet complete, since 1974 was the year when c-quark was to be discovered.
[6] Their discovery lead to them winning 1980's Nobel Prize.

satisfied. One of them is the existence of CP violation during the first moments after the Big Bang. The only explanations that don't involve CP violation rely on the assumption that the matter-antimatter imbalance was present since the beginning, however there is no scientific proof for such a case. Since the Big Bang produced equal amounts of matter and antimatter and if we make the assumption that CP is conserved, every particle would have been totally cancelled by it's antiparticle and Universe would be nothing more than a sea of radiation, totally free of matter. Since this is not the case, CP Symmetry violation is believed to exist since the Big Bang making physical laws act differently for matter and antimatter.

1.2 The Strong CP Problem

QCD is the theory describing the strong interactions between quarks and gluons. As explained in the preceding section of Chapter 1, since QCD includes three generations of quarks that have a CP-violating complex phase θ, CP Symmetry in the strong sector is to be violated.

In particle physics, the "Strong CP Problem" consists of the unknown reasons that don't allow QCD to manifest any such a violation of the CP Symmetry.

Electroweak theory has been proved to be a CP violating theory. But, unlike the Electroweak theory where the gauge fields couple to chiral currents constructed from the fermionic fields, gluons couple to vector currents. Also, there has been none experimental manifestation of any CP violation in the strong sector. However, such a violation ought to exist since the QCD Lagrangian contains the so-called θ-term which is CP violating:

$$\mathcal{L} = -\frac{1}{4}F_{\mu\nu}F^{\mu\nu} - \frac{n_f g^2 \theta}{32\pi^2}F_{\mu\nu}\tilde{F}^{\mu\nu} + \bar{\psi}(i\beta^\mu D_\mu - me^{i\theta'\gamma_5})\psi$$

The value of θ can be modified via performing axial $U(1)_A$ rotations, modifications that affect the determinant of the CKM matrix M. On the other hand, if somebody takes into consideration the parameter $\bar{\theta}$ that is being defined as follows

$$\bar{\theta} = \theta + Arg\ DetM$$

then we have a new parameter invariant under $U(1)_A$ rotations. In order to achieve CP invariance, $\bar{\theta}$ has to be zero, otherwise QCD violates CP. Through experimental data and specifically through neutron's electric dipole moment we may give an upper bound for $\bar{\theta}$: $\bar{\theta}<10^{-10}$. So, now, the Strong CP-Problem may be expressed through our non-understanding of $\bar{\theta}$'s very small value.

As a conclusion, if we try the nonzero case of the $\bar{\theta}$ parameter, CP Symmetry is expected to be violated. However, this behaviour has never been experimentally observed.

1.3 Solutions to the Strong CP Problem

The Strong CP Problem has been given several solutions but three of them are the ones mostly standing out in the literature. These three solutions are briefly described below.

1. Vanishing of up-quark's mass

The Strong CP Problem could be potentially solved if one of the quarks in the Standard Model was massless. This particle has been thought to be the up-quark. This way, the particle's field enables arbitrary chiral rotations of the CP violating term $\bar{\theta}$ and eventually absorbs it. However, first order Chiral Perturbation Theory rules this scenario out through the calculation of m_u/m_d ratio, something that is phenomenologically truthful and supported by experimental evidence, which shows that all six quarks have a mass and so the problem persists. Moreover, such a solution would only transfer the problem from explaining the small value of $\bar{\theta}$ to explaining the deriving small value of the up-quark. Lately, there is some thought on higher order corrections of Perturbation Theory to enable $m_u = 0$ which causes a lot of debate inside the scientific community but no such a result can be taken into consideration for the time being since recent calculations seem to rule this possibility out.

2.Soft weak CP violation

Several models propose an alternative solution to the strong CP Problem where CP symmetry is invariant in the Standard Model but is spontaneously broken. Before the symmetry breaking, $\bar{\theta}$=0 and so CP Symmetry can be imposed on the QCD Lagrangian. All these models are difficult to help construct Grand Unification Theories (GUTs) except for one, the Nelson-Barr model. In this scenario, CP is indeed a symmetry of the Standard Model and it's violations result from the spontaneous breaking of CP at some high energy GUT scale. The model includes particles that belong in the Beyond-the-Standard-Model region (i.e. squarks, gauginos), including flavors of heavy fermions. The model produces weak CP violation at low energy scales as expected through the Kobayashi-Maskawa mechanism. However, implementing the Nelson-Barr mechanism is, in general, rather difficult in supersymmetric theories since loop corrections involving those previously mentioned Beyond-the-Standard-Model particles give large corrections to $\bar{\theta}$ unless there is a very high degree of degeneracy. This essential degeneracy may be provided by gauge mediation, which in theory is precisely the case where one might need an alternative to axions, particles that will be followingly introduced.

3. Existence of an axion.

The last –but not least- of these three solutions is the existence of a new particle, the axion. It was postulated by R. Peccei and H. Quinn and it is considered to be the most elegant of the solutions to the Strong CP Problem. Briefly, Peccei and Quinn introduced a new global symmetry, the $U(1)_{PQ}$, which becomes spontaneously broken. This breaking results to the appearance of the axion. This particle's role is to "relax" the CP violating $\bar{\theta}$ parameter to zero through its field and dynamically vanish it. Axion's case will be discussed in the following chapter.

Chapter 2

THE AXION DYNAMICS

INTRODUCTION

QCD is a CP violating theory, however Nature has never exhibited such a behavior in any experiment. The reasons that prohibit such a manifestation of CP violation constitute what is currently known as "Strong CP Problem". The most elegant of the solution proposed to solve the Strong CP Problem is the one proposed by R.Peccei and H.Quinn in 1977. The basic concept behind the Peccei-Quinn mechanism is to no longer face $\bar{\theta}$ as a parameter of the theory but as a dynamic variable whose different values correspond to different vacuum states. The "correct" vacuum state which will lead to solving the Strong CP Problem is the one for which $\bar{\theta} = 0$. In order to obtain $\bar{\theta} = 0$, Peccei and Quinn postulated a new global symmetry, $U(1)_{PQ}$, which is spontaneously broken at some energy scale.

It was not long until S.Weinberg and F.Wilczek realized that an inevitable consequence of the Peccei-Quinn mechanism was the generation of a new particle, the axion, which is the Nambu-Goldstone boson of the $U(1)_{PQ}$ symmetry.

In this Chapter, the basics of the Peccei-Quinn mechanism are explained and the complete range of axion dynamics is being discussed.

2.1 The Peccei-Quinn Mechanism

The Peccei-Quinn mechanism was postulated in order to solve the so-called strong CP Problem of Particle Physics, which consist of our lack of understanding why strong interactions seem to conserve CP symmetry when QCD is believed to be a CP violating theory.

Consider the Lagrangian of QCD:

$$\mathcal{L} = -\frac{1}{4}F_{\mu\nu}F^{\mu\nu} - \frac{n_f g^2 \theta}{32\pi^2}F_{\mu\nu}\tilde{F}^{\mu\nu} + \bar{\psi}(i\beta^\mu D_\mu - me^{i\theta'\gamma_5})\psi.$$

The term $\frac{n_f g^2 \theta}{32\pi^2}F_{\mu\nu}\tilde{F}^{\mu\nu}$ gets involved in non-perturbative effects associated with QCD instantons which make the physics of QCD depend on the value of θ. Θ may be modified by axial $U(1)_A$ rotations on the CKM matrix. But, combining θ with the determinant of the CKM matrix, a new invariant under $U(1)_A$ rotations parameter arises:

$$\bar{\theta} = \theta + Arg\ DetM.$$

The best constraint on the value of $\bar{\theta}$ has been imposed by the experimental bound on the neutron electric dipole moment: $\bar{\theta}<10^{-10}$. This value is too small in the context of the QCD sector of the Standard Model.

R.Peccei and H.Quinn proposed to solve the strong CP Problem by introducing a global chiral $U(1)_{PQ}$ symmetry. They noticed that without $U(1)_{PQ}$ there is no possible way to achieve a theory where all fermion masses are real and $\bar{\theta}=0$. $U(1)_{PQ}$ must be spontaneously broken at the energy scale of the symmetry, f_a, enabling the dynamical restoration of CP. This breakdown is associated with a Nambu-Goldstone boson called "axion" as S.Weinberg and F.Wilczek have predicted. If a $U(1)_{PQ}$ symmetry is present, then

$$\bar{\theta} = \theta + Arg\ DetM - \frac{a(x)}{f_a}.$$

The axion creates a new field adding another term to the QCD Lagrangian

$$\mathcal{L}_{QCD} = \mathcal{L} + \mathcal{L}_{\bar{\theta}} + \mathcal{L}_{axion}$$

where the new field is now being described by the equation

$$\mathcal{L}_{axion} = \mathcal{L}_K + \mathcal{L}_I + V_{eff}.$$

In the preceding equation, the first term represents the kinetic energy, the second one the energy deriving from the interactions of the axions and the last one the effective potential of the QCD Lagrangian. The effective potential is given by the equation

$$V_{eff}(a) = -C_a \frac{a(x)}{f_a}\frac{g^2}{32\pi^2}F_{\mu\nu}\tilde{F}^{\mu\nu}$$

where $\alpha(x)$ is the axion field, f_α the axion decay constant, C_α a model-depended constant and g the strong coupling constant. As mentioned before, the vacuum state, which solves the strong CP Problem, is the one for which $\bar{\theta} = 0$ and this is where the effective potential is minimized. So, the extrema of the potential have

to be calculated

$$\langle \frac{\partial V_{eff}(a)}{\partial a} \rangle = -C_a \frac{g^2}{32\pi^2 f_a} \langle F_{\mu\nu} \tilde{F}^{\mu\nu} \rangle = 0.$$

This way, the vacuum expectation value of the axion field $\langle a \rangle$ is

$$\langle a \rangle = -\frac{f_a}{C_a} \bar{\theta}$$

which succeeds in cancelling out the CP violating $\bar{\theta}$ parameter making the symmetry invariant. Finally, expanding V_{eff} around its minimum gives the axion mass

$$m_a^2 = \langle \frac{\partial^2 V_{eff}}{\partial a^2} \rangle = -\frac{C_a}{f_a} \frac{g^2}{32\pi^2} \frac{\partial}{\partial \alpha} \langle F^{\mu\nu} \tilde{F}_{\mu\nu} \rangle \Big|_{\langle \alpha \rangle}.$$

Since the PQ mechanism is a theoretically stable construction, it is easy to conclude that what only remains is to prove Weinberg and Wilczek true detecting the axion.

2.2 The Axion Properties

In 1978, S.Weinberg and F.Wilczek[7] proposed the existence of a new particle as a result of the Peccei-Quinn mechanism, the axion. The axion is predicted to be a neutral, pseudoscalar particle, with a light mass and weakly interactions with matter.

Consider the symmetry breaking scale of $U(1)_{PQ}$, previously denoted by f_α. In general, f_α is arbitrary due to the fact that it represents the curvature of the axion potential which has its minimum for $\bar{\theta} = 0$. Consequently, all values are allowed for f_α as long as for the axion mass and its coupling constants to several particles, since they are inversely proportional to f_α. In the following sections, the interactions of the axion with several particles are examined and it's mass is calculated.

2.2.1 Axion Interactions

Depending on the model, axions couple with gluons, photons, fermions, electrons and nucleons. Each of these interactions has to be separately examined.

2.2.1.1 Axion's interaction with gluons

The coupling of axions to gluons is the feature that distinguishes the axion from other pseudoscalar particles and is described by the interaction term in the Lagrangian, meaning

[7] S.Weinberg and F.Wilczek published separately, however "together" since Wilczek's publication is dated 7 days after Weinberg's.

$$\mathcal{L}_{aG} = \frac{a_S}{8\pi f_a} a(x) F^{\mu\nu} \tilde{F}_{\mu\nu} = \frac{g_S^2}{4\pi} \frac{g_a}{8\pi m_f} a(x) F^{\mu\nu} \tilde{F}_{\mu\nu}$$

where α_S is the fine structure constant of strong interactions. The coupling to gluons is allowed by the chiral anomaly

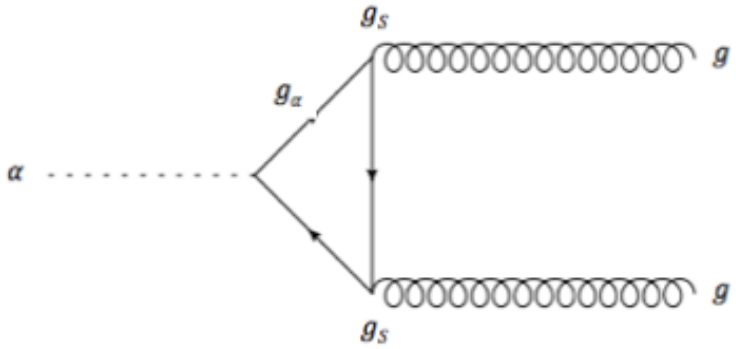

Picture 2.1: Feynman diagram of the axion-to-gluon coupling.

and provides the axion a mechanism to acquire mass. It should be mentioned that it is present in all axion models.

This coupling makes possible the mixing with pions as well, which allows obtaining the axion mass by using the expression

$$m_a = \frac{m_{\pi^0} f_\pi}{f_\alpha} \sqrt{\left(\frac{z}{(1+z+w)(1+z)}\right)}.$$

In the last equation, all known values are replaced

$$m_{\pi^0} = 135\ MeV$$

$$f_{\pi^0} = 93\ MeV$$

$$z \equiv \frac{m_u}{m_d} = 0.553 \pm 0.043$$

$$w \equiv \frac{m_u}{m_s} = 0.029 \pm 0.003$$

leading to an axion mass

$$m_a \simeq 0.60\ eV \frac{10^7\ GeV}{f_a}.$$

2.2.1.2 Axion's interaction with photons

The coupling of axions to photons is being described by the Primakoff effect, a procedure to be described in the following sections. The ability to couple with photons derives from the ability axion has to couple with gluons so it also appears in every axion model. An axion can couple to two photons, the corresponding Lagrangian being

$$\mathcal{L}_{int} = -\frac{1}{4} g_{a\gamma} F^{\mu\nu} \tilde{F}_{\mu\nu} = g_{a\gamma} \vec{E} \vec{B} \alpha(x)$$

where $g_{a\gamma}$ the axion-to-photon coupling given by the relation

$$g_{a\gamma} = \frac{a(x)}{2\pi f_a} \left| \frac{E}{N} - 1.92 \pm 0.08 \right| = \frac{a(x)}{2\pi f_a} C_\gamma.$$

E/N is a model dependent factor deriving as the ratio of the color anomaly N to the electromagnetic anomaly E. For large values of E/N the axion-photon coupling can be anhanced but for E/N ~2 it can be suppressed.

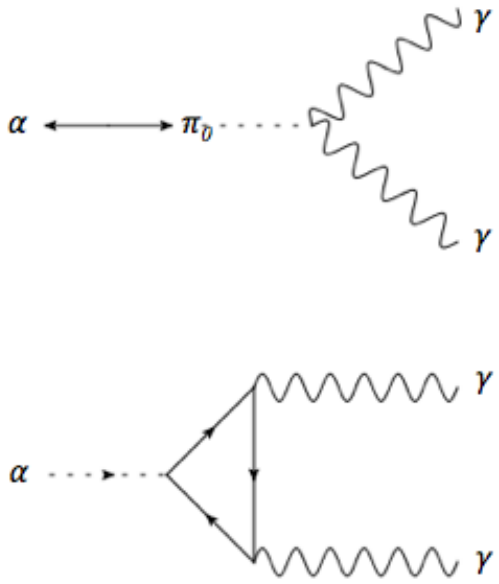

Picture 2.2: Feynman diagrams of the axion-to-photon coupling. They respectively illustrate the axion-to-pion mixing producing the generic coupling of axions to photons and the coupling via a triangle loop through fermions carrying Peccei-Quinn and electric charges.

2.2.1.3 Axion's interaction with fermions

The coupling of axions to fermions contributes to the Lagrangian with a term equal to

$$\mathcal{L}_{af} = \frac{C_f}{2f_a} \bar{\Psi}_f \gamma^\mu \gamma_5 \Psi_f \partial_\mu \alpha(x)$$

where C_f is an effective PQ charge of order unity and $g_{af} = C_f m_f / f_a$ plays the role of the Yukawa coupling with the fermion mass m_f. Followingly, the coupling to electrons and the effective coupling to nucleons can be discussed. The reason for the latter one is that no free quarks exists below the QCD scale $\Lambda_{QCD} \approx 200\, MeV$ and thus only the effective coupling to nucleons may be observed, which arises from direct axion coupling with quarks.

2.2.1.3.1 Axion's interaction with electrons

The coupling of axions to electrons is only possible if electrons carry PQ charge because, otherwise, $C_e \neq 0$. At the tree level, the contribution to the QCD Lagrangian leads to the coupling constant

$$g_{ae}^{tree} = \frac{C_e m_e}{f_a} = C_e \cdot 0.85 \cdot 10^{-10} m_a$$

where the effective PQ charge Ce depends on the axion model used. The two most important of the possible couplings of axions to electrons are being illustrated bellow:

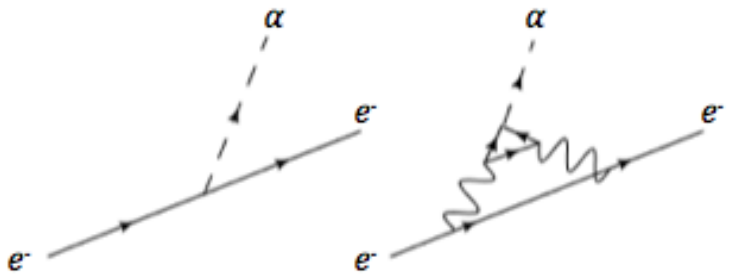

Picture 2.3: Feynman diagrams of the axion-to-electron coupling. They respectively illustrate the direct axion-electron coupling, possible in models in which fermions carry PQ charge, and the coupling of axions to electrons at one-loop level, possible even in models, which don't carry PQ charge.

2.2.1.3.2 Axion's interaction with nucleons

As mentioned before, free quarks don't exist below the QCD scale $\Lambda_{QCD} \approx 200\ MeV$. However, the coupling of axions to light quarks at tree level and the mixing of axions with pions lead to an effective axion-to-nucleon coupling, which is related to the axion mass m_α by the expression

$$g_{aN} = \frac{C_N m_N}{f_a} = C_N \cdot 1.56 \cdot 10^{-7} \cdot m_a.$$

The value of this very coupling constant depends on the model in use. So, in the context of the KSVZ model, which only assumes axion interactions with hadrons, the values to be replaced are

$$C_p = -0.39 \quad and \quad C_p = -0.04$$

and, similarly, for the DSFZ model where $C_e \neq 0$, the values to be replaced are

$$C_p = -0.10 - 0.45 cos^2\beta \quad and \quad C_n = -0.18 + 0.39 cos^2\beta.$$

2.2.2 Lifetime of Axions

One of the most important observations of the preceding section is that all axion's couplings and its mass are both inversely proportional to the PQ symmetry breaking scale f_α. This means that the larger f_α is, the smaller the axion mass and the weaker its coupling to ordinary mass becomes. This is a fact that

will be used later on.

The PQ symmetry has inherited an electromagnetic anomaly which evokes coupling of axions to two photons. Axions can decay into two photons and the lifetime of this procedure is

$$\tau_{\alpha\to\gamma\gamma} = 6.8\times 10^{24}\frac{\left({}^{m_a}/_{eV}\right)^{-5}}{\left[{}^{\left({}^{E}/_{N}-1.92\right)}/_{0.72}\right]^2}s.$$

Using the axion-to-photon coupling, the particle's lifetime can also be given as

$$\tau_{\alpha\to\gamma\gamma} = \frac{2.24\cdot 10^{14}}{g_{\alpha\gamma}^2}\left(\frac{m_a}{eV}\right)^{-3}s = \frac{0.5\cdot 10^{-3}t_U}{g_{\alpha\gamma}^2}\left(\frac{m_a}{eV}\right)^{-3}s$$

where $t_U \approx 4.35\cdot 10^{17}s$. Consequently, for a coupling of order unity, an axion of mass 0.08 eV has roughly the lifetime t_U meaning that light axions are very stable when very heavy axions have rather short lifetime.

2.3 The Visible Axion

The axion mass, as mentioned in the previous sections, is inversely proportional to the size of the Peccei-Quinn scale f_α. The size of f_α categorizes axions to two major axion model classes, the visible and the invisible axion.

The original proposition of Peccei and Quinn was that the symmetry breaking scale of the newly introduced PQ symmetry was of the order of the electroweak scale $f_{weak} \approx 250\ GeV$ producing an axion with a mass larger than 150 keV. This axion is being referred to as the visible one.

As previously mentioned, the visible axion model is defined by a symmetry breaking scale $f_a \approx 250\ GeV$. In order to obtain this value, some thoughts have to be made: In order to obtain the chiral $U(1)_{PQ}$ Symmetry, one has to introduce two Higgs-doublets, which are assumed to have non-vanishing vacuum expectation values (VEV) λ_1 and λ_2. Then, the symmetry breaking scale is calculated as

$$f_a = \sqrt{\lambda_1^2+\lambda_2^2} = \left(\sqrt{2}G_F\right)^{-1/2} \equiv f_{weak} \approx 250\ GeV,$$

where G_F denotes the Fermi coupling constant. Through standard algebra methods, the axion mass is calculated as

$$m_a = N\left(x+\frac{1}{x}\right)\frac{\sqrt{z}}{1+z}\frac{f_\pi m_\pi}{f_\alpha} = 25N\left(x+\frac{1}{x}\right)keV$$

where x the ratio of the two VEV with x>1, N the number of quark generations, $z \equiv \frac{m_u}{m_d} = 0.553 \pm 0.043$, $m_\pi = 135\ MeV$ and $f_\pi = 93\ MeV$. Since $N \leq 3$ and $f_a \approx 250\ GeV$ one obtains $m_a \gtrsim 150\ keV$.

Using the axion lifetime formula and assuming $\frac{E}{N} = \frac{8}{3}$, the visible axion is

$$\tau_{\alpha\to\gamma\gamma} \approx \frac{\tau_{\pi^0}}{z}\left(\frac{m_{\pi^0}}{m_a}\right) \approx 0.7\cdot 10^{-5}\left(\frac{1\ MeV}{m_a}\right)^5 s \approx 0.1\ s$$

where the calculated value $m_a \gtrsim 150\ keV$ was used. For axions heavier than 1 MeV, there is the possibility of the axion decaying into an electron-positron pair, thus the lifetime becomes much shorter as calculated with the formula

$$\tau_{\alpha\to e^+e^-} = \frac{8\pi f_a^2 x^2}{m_a^2\sqrt{m_a^2 - 4m_e^2}}.$$

For an axion mass around a few MeV and $x \approx 1$, the lifetime becomes almost $10^{-8} - 10^{-9} s$, which is significantly shorter than the 0.1 s calculated before.

However, the visible axion was quickly ruled out by a combination of astronomical arguments and direct experimental searches. On the first hand, axion emission and its effect on stellar evolution of red giants and on the other hand, laboratory experiments searching for rare decays of Kaons quarkonia eliminated the existence of visible axions.

2.4 The Invisible Axion

Since the symmetry breaking scale f_α is in principle arbitrary, one can choose a value much larger than the electroweak symmetry breaking scale in order to distance itself from the visible axion model. This would mean a much weaker coupling and a smaller mass than the visible axion. Consequently, the axion to be studied is known as the "invisible" one.

There exist two main models of invisible axions. The first one is the so-called KSVZ model (Kim-Shifman-Vainshtein-Zakharov model) and its most important characteristic is that ordinary matter particles don't carry PQ charge. The second one is the DFSZ model (Dine-Fischler-Srednicki-Zhitnitskiĭ model) where particles carry PQ charge. These two models are followingly explained.

2.4.1 The KSVZ model

J. E. Kim, M. A. Shifman, A. I. Vainshtein, and V. I. Zakharov suggested in 1979 and 1980 respectively the first model for invisible axions, the so-called KSVZ model. This model suggests that the PQ mechanism decouples completely from ordinary particles. This means that, at low energies, interactions between axions and matter or radiation only occur via the axion gluon coupling via en exotic heavy quark carrying PQ charge (the only particle which carries PQ charge in the model) when ordinary fermions don't carry PQ charge. For this reason, axions deriving from the KSVZ model are called "hadronic" axions. The new exotic particle, which is introduced, is a heavy quark Q and couples to a complex scalar field σ, which doesn't participate in weak interactions. This field has a large expectation value, proportional to f_α, the mass of Q is of the order hf_α and h is the Yukawa coupling.

Although the axion would couple mostly to the new heavy quark, it would still mix with the light quarks due to the color anomaly. It couples to nucleons

and the effective PQ charges are

$$C_p = -0.39 \text{ and } C_n = -0.04$$

so that the coupling for each one of the nucleons is

$$g_{ap}^{KSZV} = \frac{C_p m_p}{f_a} = -6.01 \cdot 10^{-8} m_a eV^{-1}$$

$$g_{an}^{KSZV} = \frac{C_n m_n}{f_a} = -0.69 \cdot 10^{-8} m_a eV^{-1}.$$

The coupling of axions to photons can be calculated with the formula

$$g_{a\gamma} = \frac{a(x)}{2\pi f_a}\left|\frac{E}{N} - 1.92 \pm 0.08\right| = \frac{a(x)}{2\pi f_a} C_\gamma$$

though different types of KSZV axion models suggest different values of E/N either suppressing or enhancing the coupling via the Primakoff effect, as mentioned in §2.2.1.2.

2.4.2 The DFSZ model

A. P. Zhitnitskiĭ, M. Dine, W Fischler and M. Srednicki suggested in 1980 and 1981 a new axion model, the so-called DFSZ model for axions. Here, the axion is connected to a SU(2)×U(1) singlet field σ with a large expectation value. The fundamental fermions are the ones carrying the Peccei-Quinn charge and, therefore, there is no need for the introduction of exotic quarks.

In the DFSZ model, axions can couple to electrons at tree level since the later carry the effective PQ charge

$$C_e = \frac{cos^2\beta}{N_f}$$

where N_f is the number of families and $cos^2\beta = x^2/(x^2+1)$ where x is the ratio of the VEVs of the Higgs doublets as defined in the previous section. So, the coupling constant can be obtained from the following formula

$$g_{ae}^{DFSZ} = 0.85 \cdot 10^{-10} m_a \frac{cos^2\beta}{N_f} eV^{-1} = 0.28 \cdot 10^{-10} m_a cos^2\beta eV^{-1}$$

where N_f=3 has been used. Axions also couple to nucleons. The effective PQ charge of proton and neutron are

$$C_p = -0.10 - 0.45 cos^2\beta$$

$$C_n = -0.18 + 0.39 cos^2\beta.$$

However, C_p and C_n values vary from the one DFSZ model to the other. Finally,

axions couple to photons as well. If one uses the value $^{E}/_{N} = {}^{8}/_{3}$, the coupling obtained is

$$g_{a\gamma}^{DFSZ} \approx -0.74\frac{a}{2\pi f_a}.$$

2.5 The Solar Axion

Axions are believed to be produced in the core of the Sun via the Primakoff effect. This axion is being referred to as the "solar" axion and its detection is the objective of the CAST experiment running in CERN. This section aims to introduce the reader in the solar axion dynamics. The production method is being stated, several important magnitudes are being calculated and the detection method is being discussed.

2.5.1 Production of the Solar Axion

Axions can be produced in the core of stars. There, temperatures and density of matter are extremely high and allow the conversion of blackbody photons with energies in the keV range into a non negligible amount of axions. This virtual photon is provided by the strong electromagnetic field the charged particles in the plasma produce. This is the Primakoff effect, which can be written as

$$\gamma + Ze \rightarrow Ze + a$$

and illustrated through the corresponding Feynman diagram

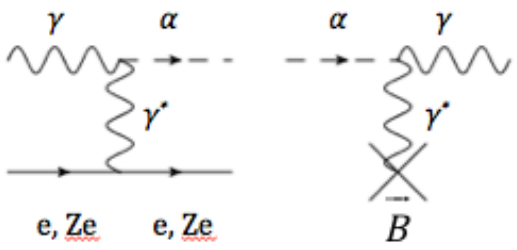

Picture 2.4: Feynman diagrams of the Primakoff effect and the inverse Primakoff effect respectively. The first one is being used in order to produce axions in the core of the Sun, the second one in order to convert axions back to photons so they can be experimentally detected.

In non-relativistic conditions, electrons and nuclei can be considered heavy in comparison to the energies of the surrounding photons and to the energies of the generated axions as well. The differential cross section of the Primakoff effect is in this case given by

$$\frac{d\sigma_{\gamma\to\alpha}}{d\Omega} = \frac{g_{\alpha\gamma}^2 Z^2 \alpha}{8\pi} \frac{\left|\vec{p}_\gamma \cdot \vec{p}_\alpha\right|^2}{\vec{q}^4}$$

where the axion and photon energies are taken to be equal and the momentum transfer is given by $\vec{q} = \vec{p}_\gamma - \vec{p}_a$. The minimum required momentum transfer is

$$q_{min} = \frac{m_a^2}{2E_a}$$

that, for $m_a \ll E_a$ yields a total cross section of

$$\sigma_{\gamma\to\alpha} = g_{\alpha\gamma}^2 Z^2 \left[\frac{1}{2} ln\left(\frac{2E_a}{m_a}\right) - \frac{1}{4}\right].$$

The cut-off of the long-range Coulomb potential in a plasma is due to screening effects resulting in an additional factor of the differential cross section such that

$$\frac{d\sigma_{\gamma\to\alpha}}{d\Omega} = \frac{g_{\alpha\gamma}^2 Z^2 \alpha}{8\pi} \frac{\left|\vec{p}_\gamma \cdot \vec{p}_\alpha\right|^2}{\vec{q}^4} \frac{\vec{q}^2}{\kappa^2 + \vec{q}^2}$$

where κ^2 is the Debye-Hückel scale given by

$$\kappa^2 = \frac{4\pi a}{T_\odot} \sum_j Z_j^2 n_j.$$

In the last formula, $T_\odot$ denotes the temperature in the plasma of the solar core, α is the fine-structure constant and n_j represents the density of charged particles carrying the charge $Z_j e$. At the solar core, κ=9 keV and $\kappa/T = 7$, a number constant throughout the Sun. The decay rate $\Gamma_{\gamma\to\alpha}$ has been calculated as

$$\Gamma_{\gamma\to\alpha} = \frac{T_\odot \kappa^2 g_{\alpha\gamma}^2}{32\pi^2} \frac{\left|\vec{p}_\gamma\right|}{E_\gamma} \int d\Omega \frac{\left|\vec{p}_\gamma \cdot \vec{p}_\alpha\right|^2}{\vec{q}^2(\kappa^2 + \vec{q}^2)}$$

Performing the integration and using all the values available ($T_\odot = 15.6 \cdot 10^6 K, E_\gamma \approx 4keV, p_\gamma = E_\gamma = E_a, p_a = \sqrt{E_a^2 - m_a^2}$) and assuming small axion masses when compared to their energy, one concludes to the formula

$$\Gamma_{\gamma\to\alpha} = \frac{T_\odot \kappa^2 g_{\alpha\gamma}^2}{32\pi} \left[\left(1 + \frac{\kappa^2}{4E^2}\right) \ln\left(1 + \frac{4E^2}{\kappa^2}\right)\right].$$

Another interesting calculation is the one referring to the axion flux expected at Earth. There are two different models calculating this magnitude. The first one was constructed by K. Van Bibber, P.M. McIntyre, D.E. Morris, and G.G. Raffelt who used the standard solar model developed by J. N. Bahcall, W. F. Huebner, S. H. Lubow, P. D. Parker, and R. K. Ulrich. K. Van Bibber and his colleagues obtained the axion flux formula

$$\Phi_a = 3.54 \cdot 10^{11} \left(\frac{g_{a\gamma}}{10^{-10} GeV^{-1}}\right)^2 cm^{-2} s^{-1}.$$

The axion luminosity using the standard model previously mentioned is

$$L_a = 1.7 \cdot 10^{-3} \left(\frac{g_{a\gamma}}{10^{-10} GeV^{-1}}\right)^2 L_{\odot}$$

where $L_{\odot}$ is the solar photon luminosity. The second model derived as a consequence of Bahcall and Pinsonneault's updated solar molar that was published in 2004 and finally re-evaluated axion parameters as

$$\Phi_a = 3.75 \cdot 10^{11} \left(\frac{g_{a\gamma}}{10^{-10} GeV^{-1}}\right)^2 cm^{-2} s^{-1}$$

$$L_a = 1.85 \cdot 10^{-3} \left(\frac{g_{a\gamma}}{10^{-10} GeV^{-1}}\right)^2 L_{\odot}.$$

Comparing these two sets of parameter values, one can conclude to the result that there are fairly small differences between the two models, differences that are not severe enough to be given more attention.

However, everything discussed above has to be subjected to constraints induced by the Sun itself. As it can be easily understood, every axion escaping the Sun would increase the consumption of nuclear fuel and since Sun has lived through half of its Helium-burning phase, its solar axion luminosity should not exceed the solar photon luminosity. Moreover, when investigating the interior of the Sun using precision helioseismology, someone has to automatically exclude axionic solar models with $g_{a\gamma} > 10^{-9} GeV^{-1}$ from theory. This implies that the axionic luminosity L_a should not exceed 10-20% of the solar luminosity. Furthermore, constraints are being imposed by the solar neutrino flux. As mentioned before, axions escaping the Sun increase the consumption of nuclear fuel something that results into a rise in temperature and an increase of neutrino fluxes. In order to have an axion-loss model compatible with the observed neutrino fluxes from the Sun, a coupling constant $g_{a\gamma} \lesssim 5 \cdot 10^{-10} GeV^{-1}$, which corresponds to $L_a \lesssim 0.04 L_{\odot}$ is needed.

Moreover, another parameter that affects theory is the fact that axions, in order to be detected, have to actually be able to escape the Sun. In order to do so, their mean free path (MFP) has to be larger than the Sun radius. With a temperature around T=1.3 keV and κ≈9 keV at the core of the Sun, the MFP of the axion, λ_a, is calculated as

$$\lambda_a \approx 6 \cdot 10^{24} g \left(\frac{g_{a\gamma}}{10^{-10} GeV^{-1}}\right) cm \approx 8 \cdot 10^{13} g_{10}^{-2} R_{\odot}$$

where $g_{10} = {}^{g_{a\gamma}}/_{10^{-10} GeV^{-1}}$. Thus, if axions where to be reabsorbed in the Sun and not escaping it, the coupling constant $g_{a\gamma}$ would have to be larger than the observed CAST limit by a factor of 107. Even if we consider such a possibility, reabsorbed axions would influence the solar structure since they would be considered to interact strongly with matter, at least stronger than photons. In such a case, the energy transfer rate in the Sun would be extremely accelerated and the solar structure would be dramatically altered making reabsorption an

unlikely eventuality.

2.5.2 Probability of Axion-to-Photon conversion

Axions, as discussed, are expected to be produced in the solar core through the Primakoff effect and since they are proven to be able to escape the Sun, they are expected to reach Earth. In order for experiments to be able to detect axions, one can propose to reverse its production's method converting an axion to a real photon through the inverse Primakoff effect. This is the case for the CAST experiment.

The expected signal at an axion helioscope such as the CAST depends on the number of axions converted to photons at the magnetic region. This conversion is only effective when the polarization of the outcoming photon is parallel to the magnetic field, which needs to be transversal to the propagating axion wave. The wave equation for particles propagating along the z-axis in a transverse magnetic field B is given by

$$i\partial_z \begin{pmatrix} A \\ a \end{pmatrix} = \begin{pmatrix} \frac{E_a - m_\gamma^2}{2E_a - i\Gamma/2} & \frac{g_{a\gamma}B}{2} \\ \frac{g_{a\gamma}B}{2} & \frac{E_a - m_\gamma^2}{E_a} \end{pmatrix} \begin{pmatrix} A \\ a \end{pmatrix}$$

where A is the parallel to B amplitude of the photon field component, B is the component of the magnetic field transversal to the propagation wave, Γ is the inverse absorption length for X-rays in the media and m_γ is the effective photon mass in the, which can be expressed in natural units as

$$m_\gamma = \omega_p = \sqrt{\frac{4\pi\alpha n_e}{m_e}}.$$

In the former formula, N_e is the electron density of the buffer gas that is related with the mass density by the relation

$$n_e = Z\frac{N_A}{W_A}\rho$$

Z is the corresponding atomic number and W_A is the atomic weight. If someone wants the effective photon mass as a function of the buffer gas density, the following formula arises

$$m_\gamma \simeq 28.77\sqrt{\frac{Z}{W_A}\rho\left[\frac{g}{cm^3}\right]}\,eV$$

where the atomic weight is now expressed in $^{g}/_{mol}$.

The conversion probability of axions to photons travelling through a transversal and homogenous magnetic field B over a total coherence length L derives using first order perturbation theory and can be written as

$$P_{a\to\gamma} = \frac{\left(g_{a\gamma}\, BL/2\right)^2}{L^2\left(q^2 + \Gamma^2/4\right)}\left[1 + e^{-\Gamma L} - 2e^{-\Gamma L/2}\cos\left(qL\right)\right]$$

where the absolute momentum transferred between the real photon in the medium and the axion, q, is calculated by

$$q = \left|\frac{m_a^2 - m_\gamma^2}{2E_\alpha}\right|.$$

The probability conversion given above can be reformulated and expressed in terms of more suitable experimental units

$$P_{a\to\gamma} = 1.6278 \cdot 10^{-17}\left(\frac{BL}{B_{cb}L_{cb}}\right)^2\left(\frac{g_{a\gamma}}{10^{-10}GeV^{-1}}\right)^2 \mathcal{M}(q,L)$$

where the normalizing factor arises from using the nominal CAST magnetic field intensity $B_{cb} = 8.802T$ and coherence length $L_{cb} = 9.26m$, while $\mathcal{M}$ is a term which quantifies the coherence of the interaction for a given axion mass m_α at given detection conditions imposed by the buffer medium at the magnetic region which fixes m_γ and Γ

$$\mathcal{M}(q,L) = \frac{1}{L^2\left(q^2 + \Gamma^2/4\right)}\left[1 + e^{-\Gamma L} - 2e^{-\Gamma L/2}\cos\left(qL\right)\right].$$

When a buffer gas is absent, the latter formula is reduced to the following one

$$\mathcal{M}(q,L) = \frac{2}{(qL)^2}1 - [\cos\left(qL\right)]$$

As it is easily shown, what the presence of a buffer gas aims for is the recovery of the conversion probability for axion masses higher than $m_a \gtrsim 0.02eV$. This fact is used by helioscope experiment searches and allows to cover a full axion mass range by measuring overlapping mass resonances produced by increasing the buffer gas density by small quantities. Thus, this technique for covering wide mass ranges requires long data taking periods due to the short axion mass coverage of a single resonance given by a fixed density in the magnetic bores of the CAST experiment.

2.5.3 Number of expected photons

The formula giving the number of photons which are expected from axion-to-photon conversion in a magnetic field, N_γ, as a function of the axion mass and the pressure of the buffer gas is the following

$$N_\gamma = \int \frac{d\Phi(E_\alpha)}{dE_\alpha} P_{a\to\gamma}(E_\alpha)\varepsilon(E_\alpha)\Delta t A dE_\alpha$$

where A and ε(E_α) are respectively the detector area and efficiency and Δt is the exposure time.

Chapter 3

THE CAST EXPERIMENT

INTRODUCTION

The detection of Axion, the particle described in the previous sections, has been a riddle for Particle Physicists. One of the pioneering experiments aiming to detect it is the CAST experiment, an experiment running sponsored by CERN, the European Organization for Nuclear Research, which is located in Geneva, Switzerland. CAST is sited near the French borders, at Ferney-Voltaire, in LHC's Point 8. It is a helioscope constructed with a magnet initially built for the LHC project that runs during sunrise and sunset dating data for 1.5 hour each run. In the following Chapter, the apparatus and all it's components are being thoroughly described.

3.1 The CAST magnet

The CAST experiment uses a decommissioned superconducting LHC prototype dipole magnet 9.26 m long, which provides a magnetic field of 9 T. The magnet is made of superconducting Niobium-Titanium (NbTi) and is composed of two straight beam bores (the first generation of magnets for the LHC was straight, not bending as the ones finally used to construct the collider) of 43 mm in diameter each, which results in a cross sectional area of $A_{cb} = 14.52 cm^2$. A graph of the magnet's cross section can be followingly seen.

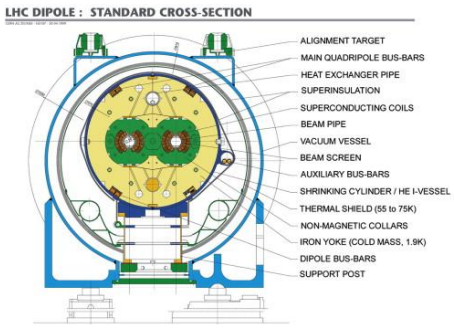

Picture 3.1: The cross section of the prototype superconducting LHC magnet.

It is installed on top of a moving platform, enabling the whole set-up to move 80° horizontally (±40° around "parking" position) and 16° vertically (±16° around "parking" position). The steering of the magnet it is controlled by a tracking system software using an internal coordinate system. The tracking system is periodically checked in order to assure that the magnet is following the Sun core with the required precision. The movement of the apparatus is constrained by the magnet weight and size (the whole construction is estimated to weigh over 50 tn) but also by the numerous connections to the cryogenics' system, the vacuum system and the pumps. This platform holds most of the weight of the Magnet Feed Box side (MFB). The weight of the Magnet Return Box is born by two oversized screws. A graph showing the magnet set-up is the following.

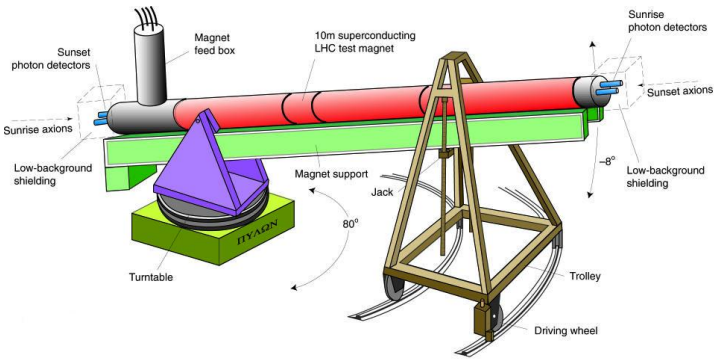

Picture 3.2: A graph showing the basic parts constructing the CAST experiment apparatus.

In order to be able to reach an intensity of magnetic field of 9 T, the magnet has to be operated in superfluid helium in a temperature of 1.8 K, using a current of 13 kA. The following two pictures demonstrate the magnetic field produced by an LHC superconducting dipole magnet.

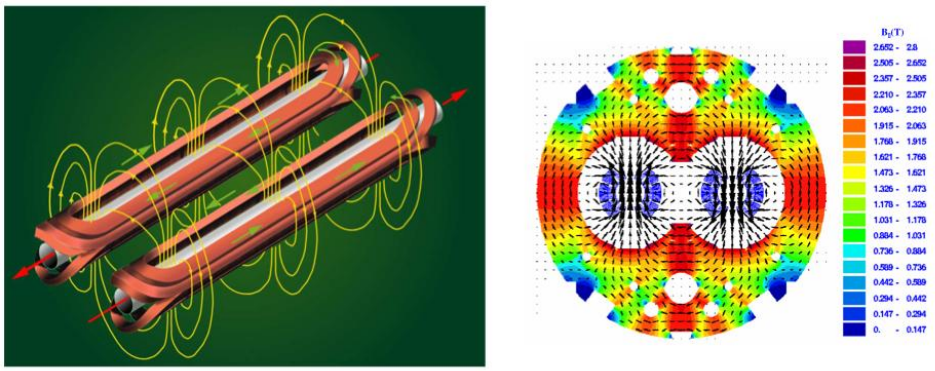

Picture 3.3: The magnet field overlength and at the cross section of an LHC superconducting dipole magnet.

In order to achieve such a cooling of the magnet, a whole cryogenic plant and a pumping group are used. The cryogenic and electric feed is done through the MFB at the side of the magnet near the platform. There, four large section cables are connected to the magnet in order to provide it with the high intensity current. However, the Joule effect produces an important heating of the cables. Thus, they are protected by a continuous water flow in order to quickly dissipate this heating.

Picture 3.4: The cables connected to the magnet, surrounded by a cooling system.

Apart from these cables, the quench recovery system has been installed at the same place. A quench is a really interesting phenomenon, which occurs when the magnet is being subjected to a sudden change of its superconducting properties leading to its normal conductive state. Then, the magnet temperature increases rapidly, leading to an increase of the pressure inside the dipole. In order to help the cryogenic set-up avoid any possible damage, a fast discharge of the current is triggered along with the closing of the liquid helium supply valve. Besides real quenches also fake quenches might occur, triggered by false warning signals of monitored quantities to detect real quenches.

Picture 3.5: A quench in CAST experiment.

The cooling of the magnet is being done in a primitive level with the help of a liquid nitrogen flow that cools down the system to about 77 K. Then, the superfluid helium circuit, constructed entirely of cryogenics from the former Large Electron Positron Collider that are no longer needed, undertakes to reach the 1.8 K needed. Moreover, a fine structure vacuum system is being used all around the magnet bore so that the cold parts of the magnet are insulated and also so that the transmission of X-rays deriving from the inverse Primakoff effect is increased.

The idea behind the magnet is simple. The magnet aligns with the Sun twice a day, during sunset and sunrise, for about 1.5 hour each time. The magnetic field provides the conditions for the conversion of axions that have entrained into the bores back to photons via the inverse Primakoff effect when the magnetic field is transversal to the direction of axions propagation. Both bores of the magnet are covered in both ends by high performance detectors, which are being subjected to continuous implementations so that their sensitivity and stability are upgraded.

3.1.1 The Vacuum System

An assembly of pumps and valves, which are used to evacuate the bore, is supporting the CAST magnet set-up. Four gate valves (VT1, VT2, VT3 and VT4)

are used in all four pipes' ends to separate the magnet from the detectors. The following scheme graphically shows the geometry of the assembly.

Picture 3.6: Positions of the four VT_i and $V1_i$ valves of the Vacuum System.

These valves are characterized by a low X-ray transmission, thus they have to be open during data taking. However, an interlock system controlling the status of all four valves has been implemented in order these valves to automatically close when a system failure occurs so that possible damage in the magnet or the detectors can be prevented. Numerous pressure probes and their corresponding gauges that are able to send alarms in any case of pressure irregularity or breakdown of the vacuum system support this interlock system. There is also the option to choose which valves to keep open and which ones to close when one or more of the detectors are not in use due to malfunction in order to enable uninterrupted data taking using the detectors still performing as expected. Consequently, every detector has been supported by its own vacuum system in order to prevent the breaking of the bore vacuum from its end. Finally, two more valves, namely V14 and V13, have been installed in both ends of the X-ray telescope in order to protect its supersensitive optics. Both of these additional valves are to be open during data taking.

3.1.2 The Solar Tracking System

As previously discussed, the magnet has been installed on a moving platform. Two motors are enabling the movement of such a platform, one for the horizontal movement and the other for the vertical movement. The tracking software of the system is in charge of modifying the rotating motors frequency in order to keep the magnet exactly aligned with the sun during data taking or achieve the desired magnet position in all other cases.

The horizontal movement of the 50 tn magnet set-up is being done on circular rails on the floor of the experimental area, using a trolley, which bears a great amount of its weight through two oversized screws. These screws are also helping the vertical motor move the magnet in z-axis. A local reference system consisting of motor encoder values for these two motors allows the tracking software to determine the position of the magnet. The magnets' movement can also be manually controlled through the encoder's control box, which is installed on the magnet, right above the moving platform. The pictures given below show several of the systems discussed.

Picture 3.7: The vertical movement motor.

Picture 3.8: The horizontal movement motor.

Picture 3.9: The encoders' control box on the magnet set-up.

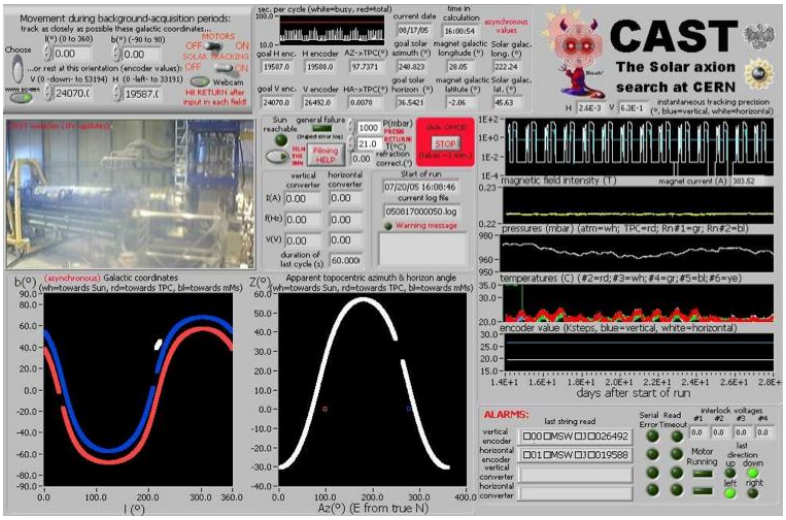

Picture 3.10: Users' interface of the tracking system software.

3.1.3 The Solar Tracking Software

One of the most outstanding features of the CAST experiment is the tracking system software which guides the magnet movement in order to keep the set-up precisely aligned with the solar core (when reachable of course) for the longest duration possible. This software is based on NOVAS, a package of subroutines provided by the U.S. Naval Observatory able to calculate various astrometric quantities. NOVAS uses the Universal Time (UT) and the coordinates of the CAST experimental area as input parameters, providing the azimuth (AZ) and zenith (ZD) angle of the Sun one minute into the future. These values are

then converted into motor encoder values and the magnet is steered to the calculated position. The software is also constantly monitoring the expected and the actual position of the magnet in order to correct every discrepancy by adjusting its speed. Regular repeated GRID measurements also are being held in order to confirm the stable and accurately operating moving system. These measurements consist of measuring the position of the magnet in a set of reference coordinates. Two lasers have also been installed on the magnet to additionally measure the relative position at some reference points.

3.1.2.2 Sun Filming

Another method of checking the pointing accuracy of the magnet during data taking is provided by Sun filming. The CAST magnet is able to directly observe the Sun twice a year, every March and September. For this purpose, the CAST experimental area has been equipped with a window, positioned in a way that Sun filming has been made possible. Sun filming is being done using two CCD cameras, a focusing system and a laser parallel to the magnet axis. The Sun needs about 5 minutes to cross the window surface, which is the actual duration of Sun filming. However, one major problem is that Sun filming is subjected to the weather conditions. However, measuring periods last for 1 week each time, which ensures most of the times at least one good measurement.

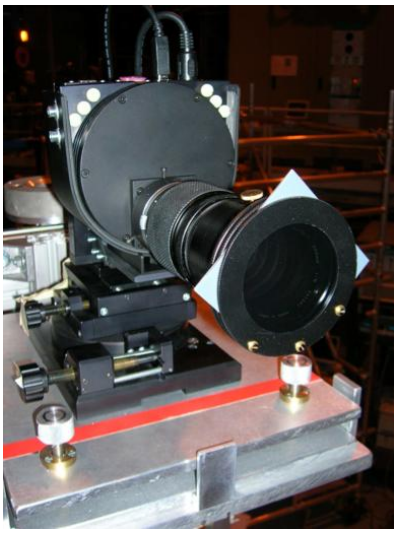

Picture 3.11: A CCD camera mounted on the CAST magnet, ready for Sun filming to start.

3.1.3 The Helium System

In Phase I (2003-2004) CAST run with its pipes under vacuum of the order 10^{-7} mbar, conditions in which the sensitivity of the experiment in the axion-photon coupling $g_{\alpha\gamma}$ was enhanced for axion masses up to m_{α}≤0.02eV. In spite of the fact that no signal of the particle was detected, Phase I succeeded to improve the current limits on the coupling constant to

$$g_{\alpha\gamma} < 8.8 \cdot 10^{-11} GeV \text{ at } 95\% \text{ CL for } m_{\alpha}\leq 0.02\text{eV}$$

which, at the time being, was the best experimental limit ever achieved. In Phase II, vacuum had to give its place to Helium in order for an enlarged axion mass range to be investigated. Since the saturated vapor pressure for ^{4}He at 1.8 K is 16.41 mbar, for higher pressures the experiment had to fill the pipes with ^{3}He. All these modifications implied consequent upgrades of the system. ^{4}He was used in Phase II operation until 2006. The experiment had to stop data taking until 2008 when the system was upgraded and data taking restarted using ^{3}He in the magnet's pipes.

Helium is the gas chosen to fill the bore pipes in order to maximize the probability of axion-to-photon conversion for a narrow mass-range in order to further improve the limit on the coupling constant for masses up to 1 eV. By continuously increasing the pressure of the gas, the CAST experiment can search in different axion mass ranges.

Since the set-up where the magnet was under vacuum mas the base for all upgrades, it seems rather logical to initiate the discussion by demonstrating it and then "upgrade" to the ^{4}He system and the ^{3}He system.

3.1.3.1 The Vacuum System

In Phase I, as previously mentioned, the magnet run with its pipes under vacuum. The complete evacuation was done using a whole set-up of pumps and valves. The system was illustrated in picture 3.3. Four valves (VT1, VT2, VT3 and VT4) were installed in all four endings of the magnet's two pipes. They were automatically closed by an interlock system in every evidence of malfunction. This interlock system was using pressure probes and their corresponding gauges in order to check the status of all valves at every given time. Except for keeping the magnet under vacuum, these valves were also used to seal an ending of the magnet when the corresponding detector had to stop data taking due to performance issues or malfunctions. This way, the experiment could continue data taking using the remaining detectors. There were also two more valves, V13 and V14, which were installed at both endings of the telescope in order to protect its optics.

3.1.3.2 The ^{4}He System

After finalizing Phase I CAST Physics Program, the system was upgraded in order to run with gas in the bore. In 2005, the experiment shutdown was used in order to design an implement a new gas system that would insert precise amounts of 4He into the pipes and at the same time control its pressure and consequently its density. The system was able to change the buffer gas density by small density steps corresponding to pressure change of 0.08 mbar at 1.8 K. Thus, the system was developed in such a way that enabled it to determine accurately the quantity of gas that was to be inserted into the magnet. The achieved accuracy reached 0.01 mbar. However, the conditions into the bore should be homogenous as well. Thus, the magnet had to be cooled by an efficient

thermal coupling of the superfluid Helium. The upgraded system is shown in the picture below.

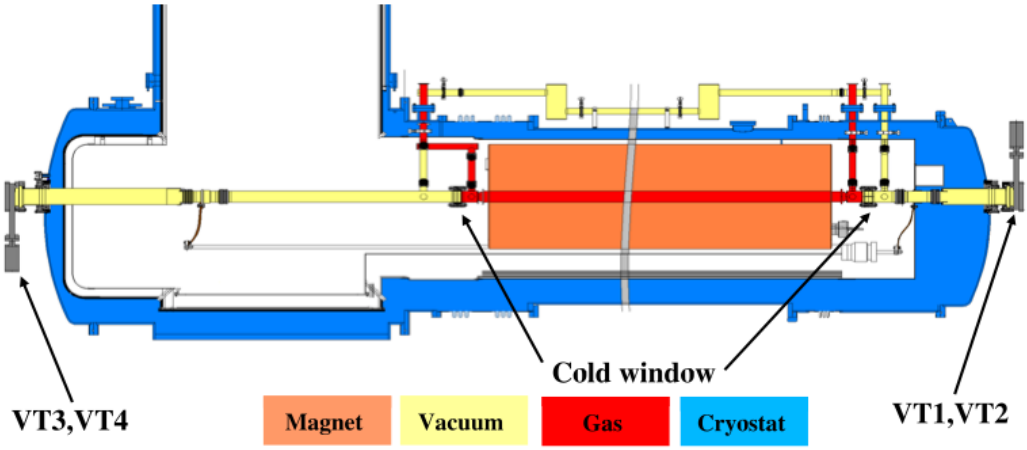

Picture 3.12: The 4He System for the CAST experiment.

The ^{4}He system had some experimental requirements to fulfill. First of all, the Helium should be absolutely confined into the cold bore. Secondly, between the inner magnet and the outer environment existed high pressure difference and thus, a resistant material should separate these two environments. For both reasons, the so-called cold windows of the CAST experiment were developed. These were four X-ray windows strong enough to withhold even the dramatic pressure changes of a potential quench of the system, on the other hand thin enough to allow X-rays in the keV range and visible light to pass through. The chosen material was 15μm thick polypropylene foil, which was mounted on a stainless steel strongback for support. However, the strongback support reduced the permeable area by almost 13% of the total area but its outstanding performance that presented only $10^{-7}\,\frac{mbar \cdot lt}{sec}$ leak and high reliability in case of a quench balanced its qualities.

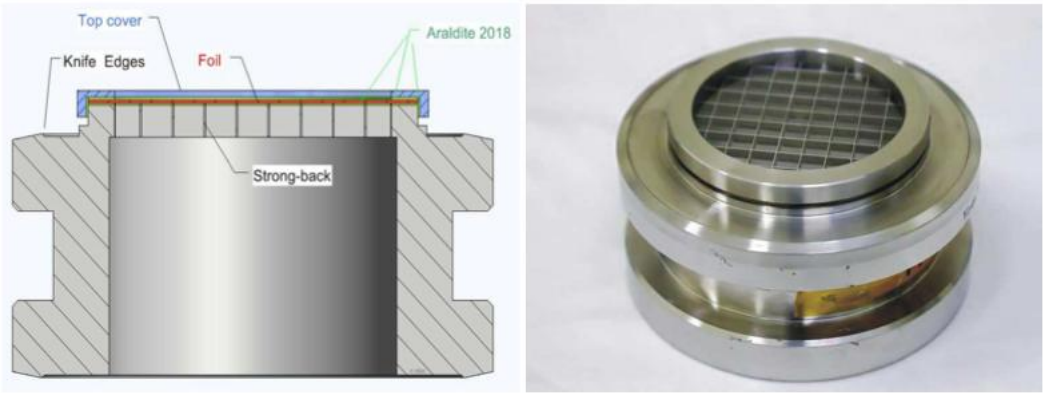

Picture x.x: The cold windows used in the CAST experiment.

Moreover, as previously mentioned, conditions inside the magnet should be homogenous. The temperature of the Helium in the cold bore within the magnetic field regions are followingly shown.

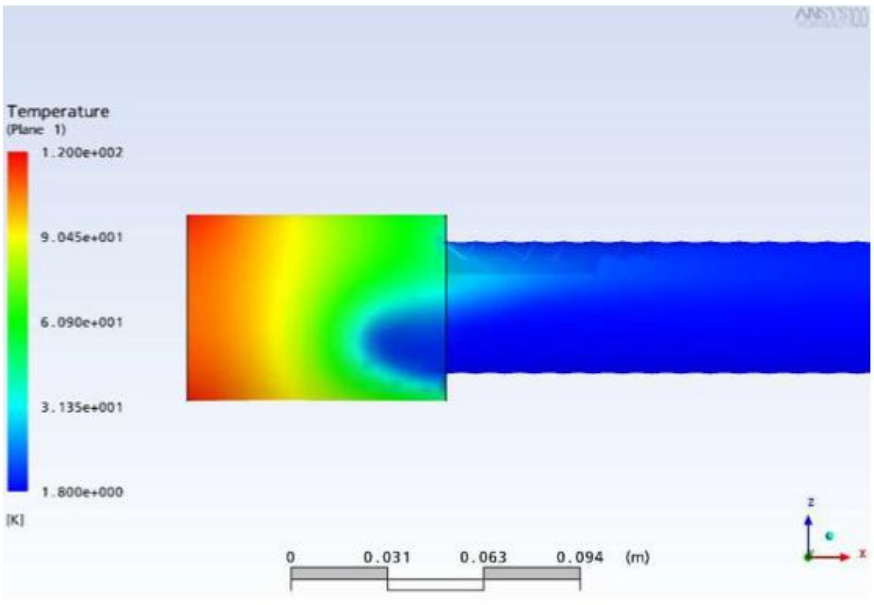

Picture 3.13: Distribution of the helium temperature in the CAST cold bore.

All experimental conditions were simulated before upgrading the system's hardware, taking into account conventional effects at the end of the magnet. When the built of the system was finalized, experimental tests were held and measurements completely agreed with the computational fluid dynamics modeling. Another condition examined was the influence of gravity on the pressure along the bore. The magnet's extreme points in the vertical movement are situations where gravitational effects cause a density gradient. However, these effects were found to be negligible when referring to ^{4}He.

3.1.3.3 The ^{3}He System

At some point, CAST experiment reached its experimental limits by reaching the saturation point of ^{4}He. It was then when the system had to be upgraded one time more so that ^{3}He could be used and higher axion masses could be accessed.

As in ^{4}He case, there were requirements to be fulfilled. First of all, the system should be as tightly sealed as possible so that no loss of the expensive gas was present. ^{3}He is a gas with a small natural abundance and demanding purification processes, factors that cause its high price. Moreover, the system should be able to accurately measure the ^{3}He inserted into the cold bore. It should also be able to protect the cold windows and guarantee the pureness of the gas avoiding any contamination. Schematically, the system is shown in the following picture.

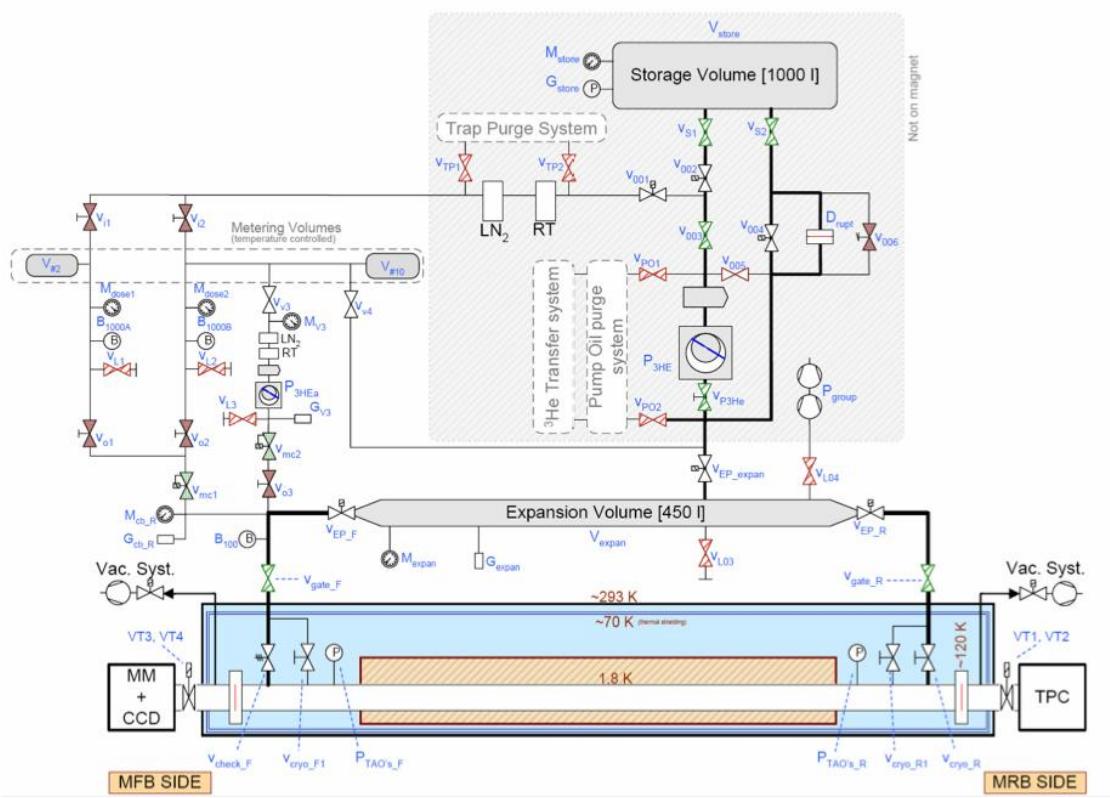

Picture 3.14: The 3He system of the CAST experiment.

In order for the ^{3}He system to fulfill its requirements and purposes there was a long period of designing every aspect of it and upgrading the 4He system. Four new parts were installed into the ^{4}He system and they are all followingly described.

First of all, a new metering system was implemented consisting of two cylindrical metering volumes of 8.58 lit the first (MV10) and 1.63 lit the other (MV2). MV10 contains gas able to increase the bore's density by ten steps while MV2 is able to increase it only by two. The thermal bath temperature is controlled by an embedded system that alerts in case water level decreases. The metering system initially was thought to consist only of MV2. However, while installing the new system it was obvious that in case of vacuum in the bore, filling the gas would take several days with duration increasing with pressure to reach, affecting the assigned days for data taking period. Thus, MV10 was also installed reducing time needed to fill the bore when totally empty.

Secondly, as previously mentioned, the system ought to guarantee the purification of the gas. Consequently, a new purging system should be built. It consists of two charcoal traps, which purify ^{3}He. The first one (RT) is at room temperature and traps oil and water vapors and the second one (LN_2) is at liquid Nitrogen temperature of 77 K purifying the gas from the remaining impurities.

Picture 3.15: The trap used in the gas purging system.

Moreover, a new expansion volume and a recovery system were installed. In previous sections, the so-called cold windows of the experiment were discussed and their sensitivity was stressed. In order to save these X-ray windows and also avoid loss of the precious gas, a safety system was implemented. In case of phenomena, which affect the cold windows, a quench is one of them, their collapse is possible. Thus, the bore got connected to an expansion volume installed right above and parallel to the bore in case its pressure increases rapidly. The valves separating both pipes from the environment (VT1, VT2, VT3 and VT4) automatically open through the quench alarm interlock activation enabling the gas to move into the expansion volume. The expansion volume has a capacity of 450 lit. In the worst-case scenario, if 140 mbars of gas at 1.8 K are inside the bore, the expansion volume constrains the maximum pressure to less than 1100 mbar presenting a safety factor of 1.2. After enabling the gas to be distributed between the bore and the expansion volume, it is recovered back to the storage volume by using a powerful pumping system that is able to simultaneously purge the gas from any contamination deriving from the pump. Afterwards, the refilling of the magnet is ready to take place again.

Finally, the status of the valves, pressure sensors and flow meters in monitored in the new 3He system by a Programmable Logic Controller (PLC). Interference between users and the software is extremely easy and rather safe due to safety parameters implemented. A screenshot of the PLC desktop is followingly given.

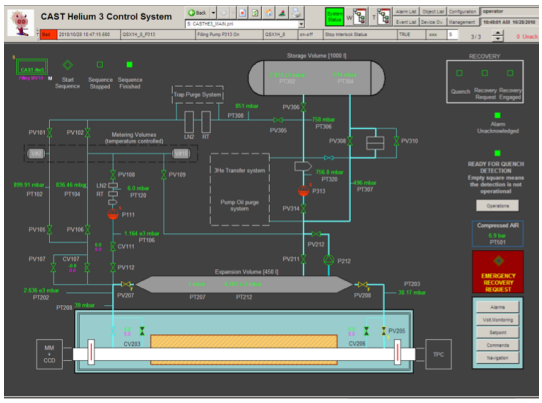

Picture 3.16: Screenshot of the PLC desktop.

All tasks able to be performed by the new 3He system (gas recovery to the storage volume, pressure step change etc.) are now automated by the PLC system.

All new systems implemented while upgrading the 4He system resulted in a system absolutely capable to react in most of the possible experimental scenarios. It is able to increase density metering possibilities, not only being able to increase the density in the cold bore but also decreasing it so that it is possible to move also back to pressure settings if it is necessary. This way, any possible scanning pattern needed can be designed. One of them is actually being used in the CAST experiment data taking procedure, where the density of the gas in the bore is increased by one step during the procedure and having the 50 tn set-up moving, completely aligned to the solar core. This way, the CAST experiment covers two density steps each day taking data for each one of them both from sunrise and sunset detectors.

3.1.3.3.1 Data Taking Routine With The ^{3}He System

In order to have a more precise picture of the CAST experiment run routine, one should keep in mind that the basic thought is taking data for 1.5 hour twice a day, during sunrise and sunset. Sunrise and sunset are not chosen for any other reason but because it is then when the Sun is low at the horizon and so the CAST magnet which is only able to move vertically from -8°to +8° is able to align. The tracking software begins calculations on when the magnet is possible to align to the Sun, motors move in full frequency until the magnet reaches the point where it is "meeting" the Sun. This point is easy to be realized by shifters on duty due to the motors stop moving. Then, the Sun approaches the meeting point as well and the frequencies of the motors are automatically modified, starting to move the magnet in order to keep it aligned to the Sun. For the next 45 minutes detectors are taking data for the first of the predefined steps. At the middle of the run, the shift leader changes the pressure setting manually for a step of 0.086-0.0114 mbar and data taking continues for 45 more minutes, until solar core and magnet lose any alignment possible. The pressure setting procedure and the stabilization of the system take only 3 minutes to be done. Then, the magnet keeps moving until it reaches its extreme point taking data from whatever can be coming from the solar corona. When reaching the extreme point, the motors are automatically starting to work at full frequencies bringing the magnet back to its parking position. Detectors are not being shut down but they are let to take background data all day long, until the next run takes place. Phase II of the CAST experiments aims to cover all pressure settings examining a range from 13.25 mbar to currently 120 mbar at 1.8 K corresponding to an axion mass of 1.15 eV.

A signal triggering protocol is being used in order to evaluate the significance of the number of tracking counts measured with respect to the mean background of the detectors for any given density step. If the signal significance of all the detectors combined exceeds the threshold imposed by the background detector statistics, this pressure step is considered to be a candidate. Then, the

assembly is being brought back to this pressure setting taking data for several runs, allowing CAST to examine the presence or not of a particle signal.

3.2 The Detectors

CAST data taking periods are being distinguished not only in terms of the gas set-up and operation but also due to the different types of X-ray detectors used. Until today, three types of detectors have been used in order to detect photons coming from axion conversion through the inverse Primakoff effect: a Time Projection Chamber (TPC), a Charged-Couple Device (CCD) and numerous MICROpattern GASeous detectors (MICROMEGAS or mM). However, only two of them have survived competition, the CCD and three MIGROMEGAS. Detectors in the CAST experiment are in the sensitivity range between 1 and 15 keV covering smoothly the energy range where the particle is expected to exist. The detector system assembled provides in every given time of the CAST experiment history the most sensitive setup with the highest discovery potential.

3.2.1 The Detectors of Phase I and ^{4}He Phase II

As thoroughly discussed in previous section, the CAST program data taking runs twice per day, during sunrise and during sunset. During sunrise, the detectors being used are the ones placed in the MFB side of the magnet. There, a MICROMEGAS and a CCD detector are installed. The CCD detector is also aligned with an X-ray focusing telescope that significantly improves the signal-to-background ratio. On the other side, the MRB one, a TPC that used to cover both pipes' ends was installed

3.2.2 The Detectors of ^{3}He Phase II

The first modification in the detectors' setup after the 3He system upgrade was to replace the TPC of the MRB side with two MIGROMEGAS detectors of the latest technology available. When compared to TPC, the MICROMEGAS detector provides higher background discrimination capabilities. The MFB side was not modified.

Every part of the detectors' system used in both phases of the CAST experiment is followingly described.

3.2.3 The CCD Detector

The CCD detector of the CAST experiment is placed at the focal plane of the X-ray telescope. It is a prototype, 280 μm thick, developed for the ESA's XMM-NEWTON mission. It has a sensitive area of 2.88 cm^2 divided into 200·64 pixels, each pixel covering a region of 150·150 μm. The effective diameter of the axion signal coming from the Sun core in the CCD chip is 19 pixels, which equals 2.83

mm. The detector operates at a temperature of −130°C, which is kept stable over time by using a Sterling cooling system. A major advantage of this type of solid state X-ray detector is the high quantum efficiency close to unity in the energy range of interest due to its very thin (20 nm) entrance window at the backside of the chip, allowing to operate the detector in vacuum without any additional windows. The good spatial resolution of the CCD chip allows to perform some pattern recognition techniques, which are used to discriminate cosmic events such as muons, and other ionizing processes. The remaining background leads to a level of $(7.5 \pm 0.2) \cdot 10^{-5}\mathrm{cm}^{-2}\mathrm{s}^{-1}\mathrm{keV}^{-1}$ in the axion sensitive range from 1 keV to 7 keV, which gives a total mean value of 0.15 counts during a full CAST solar tracking. The background level achieved by the CCD detector is partially due to internal radiation coming from the materials close to the detector. Simulations preceding the installation of the detector proposed that the contribution of natural radioactivity coming from the materials surrounding the detector could account for at most 33% of the observed background level while about almost 50% of the background is induced by environmental gammas. ^{222}Rn is usually one of the strongest sources of natural radioactivity, however, since the detector is operated in vacuum, the ^{222}Rn contribution is not important at the actual level of sensitivity.

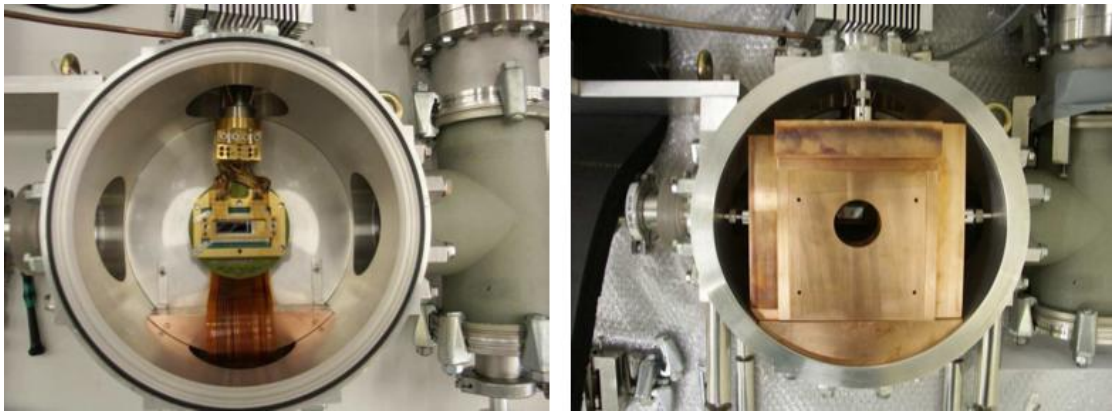

Picture 3.17: The CCD detector mounted on the bore of the CAST experiment unshielded (left picture) and shielded by 2 cm low-activity, oxygen-free copper and 2.2 cm ancient lead (right picture).

3.2.4 The X-ray Telescope

At the sunrise side of the magnet and especially at the pipe of the bore where the CCD detector is installed, a Wolter I type X-ray telescope device is placed between the detector and the pipe end in order to focus the incoming photons on the sensitive chip. This telescope is a prototype of the X-ray satellite mission ABRIXAS, which was finished in 1999. It consists of a combination of 27 nested and gold-coated parabolic and hyperbolic mirror shells with a focal length of 1600mm. The maximum aperture of the outermost shell is 163 mm while the smallest shell has a diameter of only 76 mm. The front side of the X-ray mirrors shell is divided into six sectors from which only one is used, given that the magnet bore diameter 43 mm is smaller than the sector size. The telescope efficiency of each of these sectors was fully characterized at PANTER facilities and the sector that presented better performance was chosen.

Its purpose is to focus the expected signal in a small region of the CCD chip that is specially designed to cover the X-ray energy range from 1 to 10 keV. The telescope is being kept under vacuum, at a pressure below 10^{-5} mbar in order to avoid contamination and absorption on its reflective mirror surface, which would result in a degradation of the system efficiency. The system is equipped with additional gate valves separating the magnet from the mirror optics and the optics from the CCD detector accordingly in order to insulate the mirror's system atmosphere from the rest of the experimental environment in order to avoid any damage done on the telescope. The overall performance of the X-ray optics depends on two parameters, the transmission efficiency and the spot size on the CCD chip. The use of a telescope mirror system entails a loss in signal efficiency which is counteracted by the increased significance of a smaller spot size on the detector, which concentrates a signal distributed in an area of 1452 mm^2 to a spot of about 9 mm^2, magnifying the signal to background ratio by more than a factor 100.

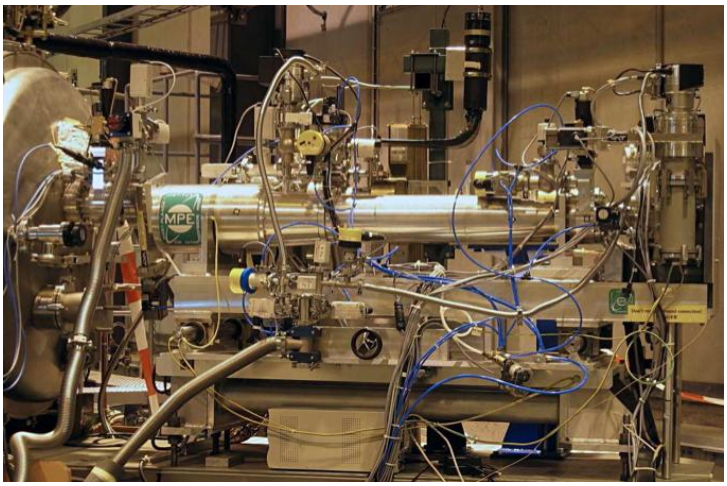

Picture 3.18: The X-ray telescope installed at the MFB side of the CAST experiment.

3.2.5 The TPC Detector

The TPC is a detector coming from the Multi Wired Proportional Chamber implemented by G. Charpack, which was the beginning of a detectors' generation based on the ionization of a gaseous medium, combined with principles of drift chambers. However, while in the MWPC there is only an amplification field, in the TPC the drift field region and the amplification field region are distinguished. Thus, the amplification region it is built between anode and cathode wires which are transversally distributed conferring a two dimensional readout to the detector. In a TPC detector, the primary interaction of the photons takes place in the central piece of the detector, which is a large gas-filled volume. There, incoming particles are being converted into free electrons via an ionization process. The electrons can then drift towards a net of anode wires. Due to the strong electric field, an avalanche process takes place, resulting in an amplification of the signal. The first coordinate can then be obtained from the

anode wire giving the signal, the second one can be obtained from the signal induced on the cathode wires and the drift time it is eventually possible to determine the third coordinate, which gives the detector its name.

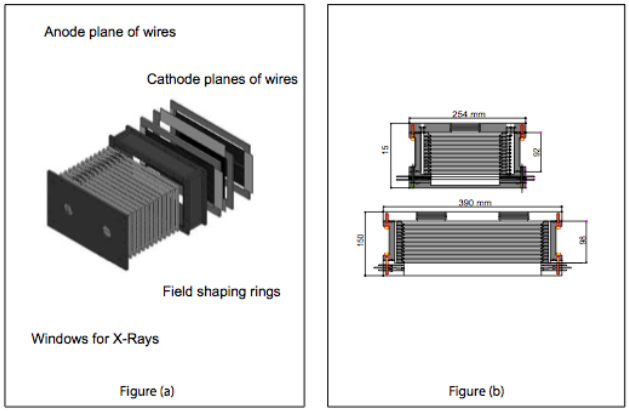

Picture 3.19: The TPC detector used in the CAST experiment.

In CAST experiment a photon coming from an axion conversion would travel through a vacuum buffer space, entering in the conversion-drift region, where it generates a photoelectron via the photoelectric effect. The photoelectron travels a short distance during which it creates ionization electrons. The electrons drift in a field of about 700 $\frac{V}{cm}$, until they reach the cathode wires and enter the amplification region where a strong field of about 5 $\frac{keV}{cm}$ causes an avalanche magnifying the signal. The cathode plane consists of 48 wires with a diameter of 100 μm each when the anode plane consists of 48 wires but of a diameter of 20 μm each. Two adjacent wires have a distance of 3mm between them, which is exactly the distance between the anode and the cathode planes. The anode plane operates at +1.85 kV and the cathode plane is grounded. The CAST TPC detector had a conversion volume of 10·15·30 cm^3 filled with a mixture of Argon (Ar) with 5% Methan (CH^4) gas at atmospheric pressure. The dimensions of the TPC section 15·30 cm^2 allow to cover both magnet bores at the sunset side of the experiment. In the front of the detector two windows, consisting of a very thin aluminized Mylar foil of about 3 μm thick stretched on a metallic strongback, are present in order to allow for X-rays coming from axion-photon conversion to pass-through. The Mylar windows are necessary because the pressure difference between the gas in the detector and the vacuum inside the magnet is about 1 atm and thus they serve as connection between the detector and the magnet bore pipe, which is in vacuum. The entire chamber is made of 1.7 cm thick low radioactivity Plexiglas, except for the electrodes, the screws and the windows. The requirement of such thin windows for reducing the signal loss, due to the X-ray transmission relation with thickness, allows some molecules to be present in the gas mixture inside the detector chamber diffuse through them due to the pressure difference between the chamber and the vacuum side, and disturbing the vacuum side of the CAST magnet bore pipes. In order to solve this problem, a differential pumping system

is necessary. The vacuum next to the detector is split in two regions ("bad" vacuum side at about 10^{-3} mbar and "good" vacuum side at about 10^{-6} mbar) by means of a thin (4 μm) polypropylene window. These volumes are pumped independently. Then, the effect of gas molecules coming from the detector towards the good vacuum side is diminished due to the lower diffusion at the polypropylene window, since the pressure difference is much lower. The TPC chamber connection to the magnet and the TPC set-up at the CAST experiment is shown below.

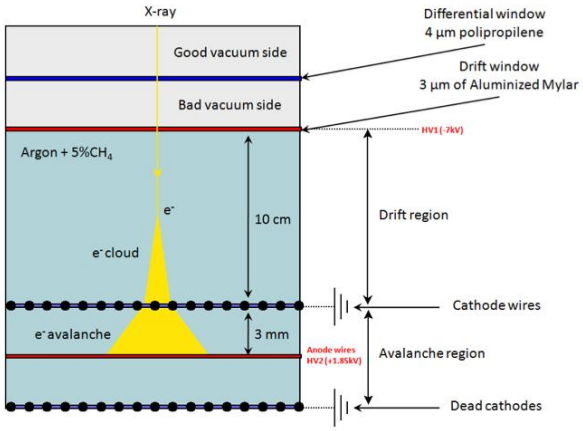

Picture 3.20: TPC functional scheme concept and set-up of the TPC detector operating in CAST.

A shielding around the TPC was designed to reduce the background level of the detector and to reduce positional background systematics mainly due to the contamination of the walls at the CAST host building, and the distance to them at the different magnet positions. The resulting shielding design was a compromise between the background reduction of the different components of the shielding and the technical constrains coming from the weight and size available for placing the shielding. From the most inner part, the shielding is composed by a copper box, 5 mm thick, which reduces electronic noise and low energy X-rays, lead bricks, 2.5 cm thick, which reduce the low and medium energy environmental γ radiation, a cadmium layer, 1 mm thick, to absorb thermal neutrons which are slowed down by the surrounding polyethylene pieces with a total thickness of 22.5cm. Thus, a PVC bag tightly covers the whole shielding allowing to reproduce a clean nitrogen atmosphere and to purge possible radon abundance around the detector. After the installation of the shielding the background reduction achieved compared to the previous data showed a reduction factor between 2.5 and 4, furthermore the previously observed discrepancies of background levels at different positions were vanished due to the shielding reduction of γ sources coming from the walls. The typical background rate of the detector after shielding reduction was about 20-60·h−1 at the energy range from 3 to 7 keV.

Historically, the TPC detector was the first detector, which took data at the CAST experiment, and it covered the vacuum Phase I and the ^{4}He Phase II of the CAST data taking program. However, the TPC was replaced by a new detector system composed by two MICROMEGAS detectors, which showed improved capabilities in background discrimination when compared to the TPC.

3.2.6 The MICROMEGAS Detectors

In CAST Phase II upgrade to the ^{3}He system, the TPC detector covering both pipes' ends at the MFB side of the magnet was replaced by two MICROMEGAS detectors of the latest technology available. This modification to the experiments' detectors assembly was done due to the technical limitation of the TPC, which had reached its wiring space limit. However, a MICROMEGAS detector already existed in the MRB side, making this particular detector type the head of the CAST detectors' assembly.

MICROMEGAS is a micropattern gaseous detector consisting of 192 conductive strips in the X-axis direction and the same amount in the Y-axis direction printed on a board. This technology allows to obtain shorter spacing in the order of less than 300 μm providing a higher spatial resolution, able to reach values lower than 60 μm at the right conditions, moreover improving the modest rate capabilities of conventional MWPC of about $103 s^{-1} mm^{-2}$. Moreover, the fact that the strips readout is built over a flat surface allowed to built shorter amplification gaps in the order of 50μm to 100μm, which provides excellent gain properties. The most robust detector structure together with the thinner amplification gap confers the detector an excellent energy resolution, below 12% FWHM at 6keV, placing the MICROMEGAS technology as one of the best candidates for use in multipurpose applications which moreover require an accurate particle identification. The higher rate capabilities of micropattern detectors, 10^7 $s^{-1} mm^{-2}$, makes them suitable to operate in applications where high-rate beams are present. Thus, MICROMEGAS detectors are consolidating in several experiments, from a neutron detector at the n-TOF beam facility to a muon tracker for the COMPASS experiment. Research and development is undergoing to introduce these detectors in future applications, as a large muon track detector for the s-LHC or as a promising candidate for studying neutrino physics at NEXT.

The MICROMEGAS detector at CAST consists of a sensitive area slightly higher than the expected cold-bore signal region of about $15 cm^2$. The MICROMEGAS operation is followingly illustrated.

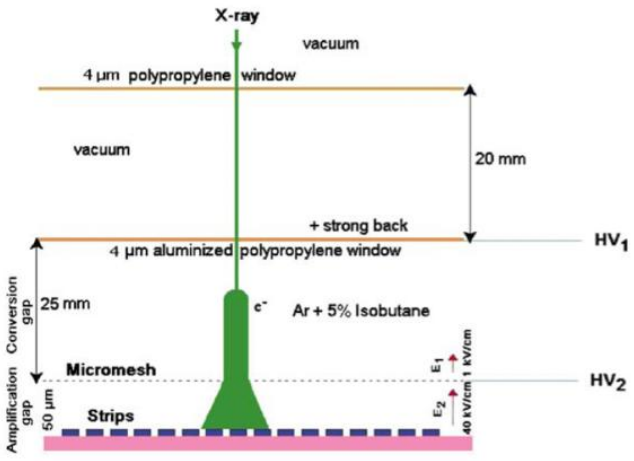

Picture 3.21: The MICROMEGAS detection principle.

After crossing a buffer space of vacuum between two windows, a photon entering the detector from the magnet aperture can produce an ion-electron pair via the photoelectric effect in the conversion-drift region. This volume is filled with a gas mixture of Argon (95%) and Isobutane (5%). The generated photoelectron can then drift due to a drift voltage of almost 1100 V for a short distance creating further ion-electron pairs. When the electrons reach the micromesh, they can enter the amplification region, where a voltage of up to almost 400 V is applied. There, an avalanche process is started due to the strong field. The grid will stop ions produced in the avalanche process from reentering the conversion region. It collects the charges of the ions and thus provides one of the readout signals. The electrons travel further till they reach the anode plane, where their signal is then collected by a structure of x-y-strips.

In contrast to the TPC detector, the amplification gap is delimited by a thin micromesh conductive grid which structure depends on the MICROMEGAS detector type. The mesh consists of 5μm copper with circular holes of 25 μm diameter and a separation distance of 50 μm. The gap homogeneity is achieved by placing precision insulating pillars between the readout plane and the mesh. The amplification field is reached by applying a high voltage at an electrode in contact with the micromesh (usually denominated as Vm or HV 2) while the strips' plane remains grounded. The short amplification distance and the surface homogeneity allows application of an amplification field of about 40 $\frac{kV}{cm}$. The 2-dimensional pattern of the strips plane provides the detector of positional sensing by measuring the total induced charge in each of the strips. A low radioactivity and cylindrical Plexiglas chamber defining a drift distance of 2.5^{-3} cm tightly encloses the MICROMEGAS readout in order to circulate argon mixtures minimizing external contamination. A thin 4 μm aluminized polypropylene window with a high X-ray transmission is placed on top the Plexiglas chamber, where the high drift voltage is applied (usually denominated as Vd or HV 1) serves at the same time as connection to the vacuum side of the magnet bore pipes. As in the case of the TPC chamber, the gas contained inside the chamber diffuses through the thin drift window towards the vacuum side of the magnet. In order to minimize this effect, a differential pumping system was implemented, separating the vacuum next to the detector by means of a 4 μm polypropylene window. A picture of the MICROMEGAS detector used in the CAST experiment is given bellow, precisely illustrating the whole set-up of the detector.

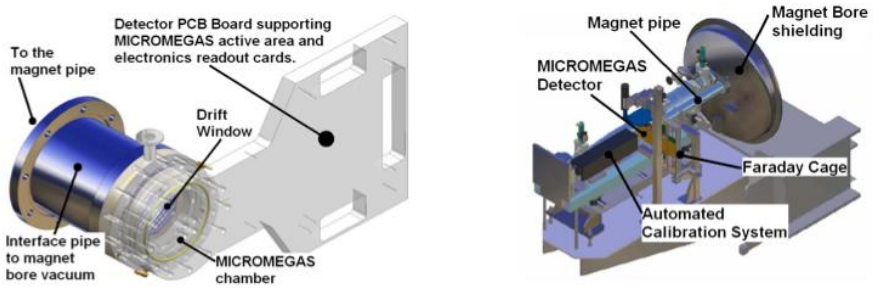

Picture 3.22: The set-up of the MICROMEGAS detector used in the CAST experiment.

Chapter 4

THE CAST PHYSICS PROGRAM

INTRODUCTION

The system described in the previous chapter can be considered, for the time being, as the most sensitive helioscope in the experimental world. However, an experiment is not over being discussed unless the scientific purpose of it is been stated. This chapter aims to fulfill this requirement of the presentation of CAST experiment and axion hunting through it. Moreover, the results of all CAST Phases are presented.

4.1 The CAST Physics Program

CAST is an experiment designed and implemented focusing on the discovery of an hypothetical particle, the axion. It consists of two discrete Phases, I and II, and three magnet set-ups, the vacuum, the ^{4}He and the ^{3}He set-up. All set-ups have already been presented. It started data taking in 2003 and has already dramatically limited the axion-to-photon coupling.

During Phase I, the magnetic field region of the prototype superconducting LHC dipole magnet was kept under vacuum, enabling to search for axions in the mass region up to 0.02 eV with very high sensitivity. However, for higher mass regions, the coherence condition is no longer fulfilled and sensitivity of CAST decreases rapidly. Phase I started data taking in 2003 and lasted until 2004. By combining the results of all detectors used, CAST improved the current limits on the coupling constant

$$g_{a\gamma} < 8.8 \cdot 10^{-11} GeV \text{ at } 95\% \text{ CL for } m_a \leq 0.02 eV.$$

Schematically, the CAST Phase I results are being illustrated in the following plot.

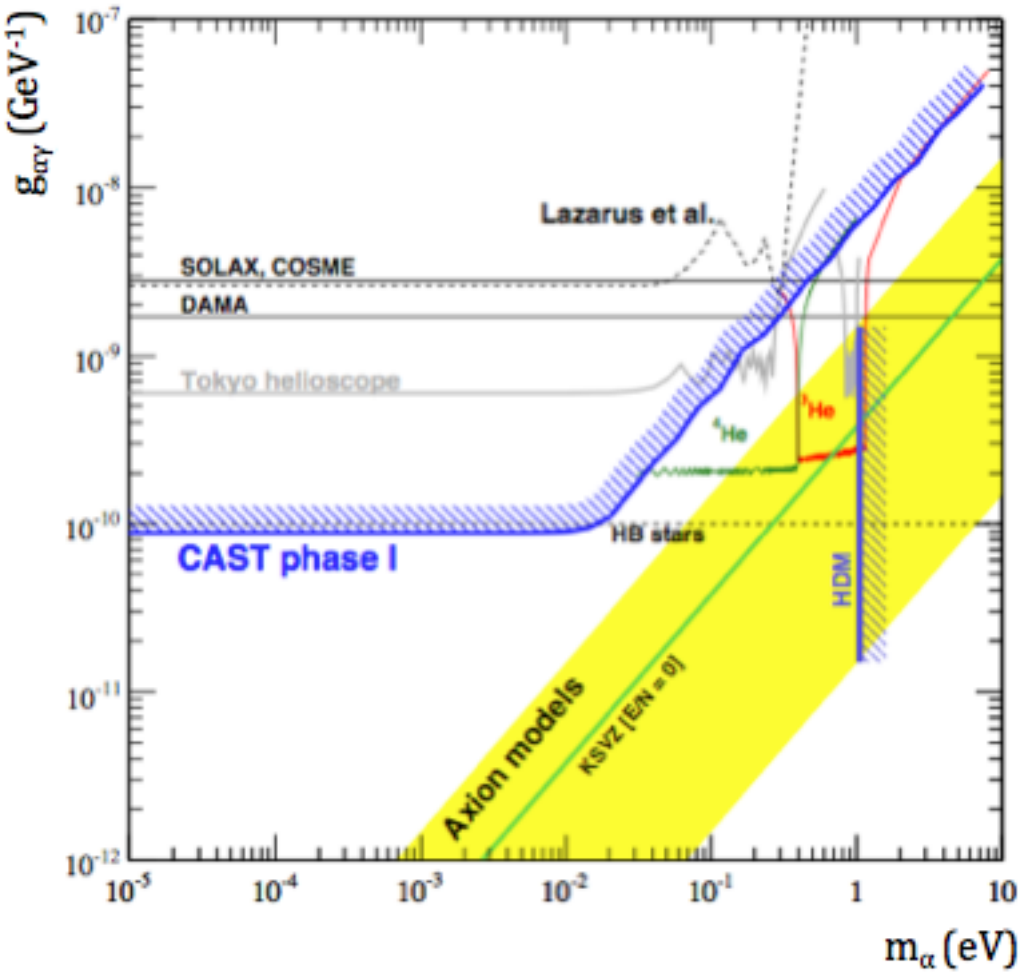

Picture 4.1: Exclusion plot for the axion-to-photon coupling relative to axion's mass as derived from CAST Phase I.

Phase II was implemented in order to be able to move the experimental procedure on, to mass regions up to about 1.2 eV. The modification of the experiment consisted primarily on the usage of a refractive buffer gas inside the cold-bore pipes. Then, while systematically changing the density of the gas at a constant temperature and thus its pressure inside the magnet, different axion masses can be studied, since each density setting restores the coherence in a narrow mass range. The step size in density inside the cold bore has been chosen in a way that consecutive settings overlap and thus an excellent and smooth coverage of the accessible mass range is provided. Two types of gases were used in CAST Phase II. First of all, ^{4}He was used during 2005 and 2006 data taking periods, scanning axion masses with high sensitivity up to about 0.39 eV, since the saturation pressure of ^{4}He at 1.8 K is 16.41 mbar. In order to stay within safety limits of the setup, CAST did not go up to this highest pressure. To reach higher masses, ^{3}He can be used, which has been done at CAST starting in 2008. Here, the saturation pressure at 1.8 K is 135.58 mbar, which extends the mass range to search for axions up to about 1.2 eV. By combining the results of all detectors used, CAST's Phase I, Phase II-^{4}He System and the first data taking period of Phase II-^{3}He System improved the current limits on the coupling constant

$$g_{a\gamma} < 2.3 \cdot 10^{-10} GeV \text{ at } 95\% \text{ CL}$$

Schematically, the previously mentioned results are being illustrated in the following plot.

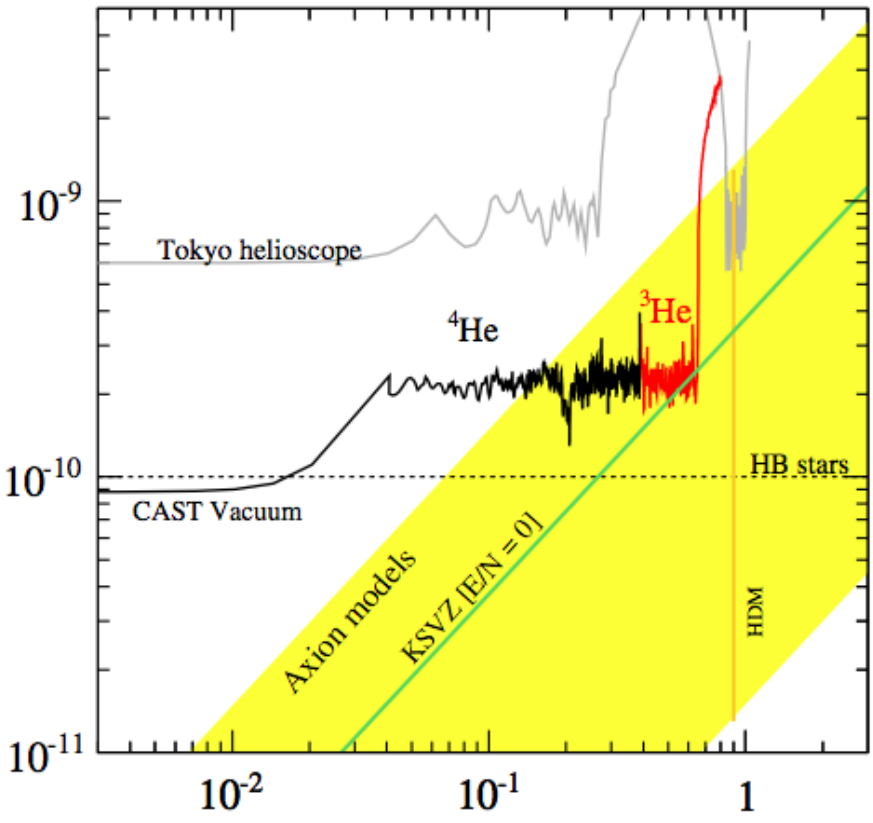

Picture 4.2: Exclusion plot for the axion-to-photon coupling relative to axion's mass as derived from the combination of CAST Phase II ^{3}He System and ^{4}He System.

CONCLUSION

A hypothetical particle, the axion, has been proposed in order to solve one of the most puzzling riddles of Particle Physics, the Strong CP Problem. The Strong CP Problem arises when QCD hasn't experimentally manifested any CP violation, despite the fact that it is considered to be a CP violating theory. The existence of the axion was proposed by R. Peccei and H. Quinn in 1977, who tried to restore order by postulating a new global symmetry, which at some scale is being broken leading to the appearance of the axion.

The axion, if existing, interacts with different particles in different ways. The coupling with ordinary matter would have some observational implications in astrophysics and cosmology which allows to constrain the axion properties in terms of axion mass and coupling strength. In particular, the existence of axions would play a role in stellar evolution, and the fact that the axion has mass places it in cosmological models as a possible candidate for dark matter, which depending on its mass could account for a dominant contribution to the total dark matter in the Universe. Moreover, axions could also be related with other physical processes of insufficient understood nature, as the solar corona heating problem or the modulation of the Earth magnetic field.

Since the existence of the axion is of such an importance, experimental searches for axions are well motivated. One of the experiments searching for axions, the CAST experiment hosted by CERN, the European Organization for Nuclear Research, uses a decommissioned prototype superconducting LHC dipole magnet as a telescope in order to search for axions coming from the Sun. It reverses the effect causing axion's birth, the Primakoff effect, by applying a powerful magnetic field of 9 T. This helioscope search was the one presented in this thesis. CAST consists of the previously mentioned magnet able to perform horizontal and vertical rotations due to its placement on a moving platform. It takes data for 1.5 hour in sunrise and sunset as well and the rest of the day takes background measurements. It has been possible for the magnet to follow the solar core through a carefully implemented tracking system consisting of hardware motors and encoders and a tracking system to. X-ray detectors of edging technology mounted on both ends of the magnet try to detect every signal possible coming from the Sun. CAST has been divided in to experimental phases with Phase I being the one where the magnet operated with its pipes under vacuum and Phase II where buffer gas was used to fill the cold bore. Phase II has also been divided to two parts, the first one being where the system used ^{4}He as a buffer gas and the second where the system was upgraded in order to operate using ^{3}He.

CAST started taking data in 2003. CAST Phase I official data taking was in 2003 and 2004. As previously mentioned, Phase I was characterized by the vacuum inside the bore's pipes. These conditions enabled the magnet to search for axion masses ≤ 0.02 eV. Phase I improved the current limits on the coupling constant to the number

$$g_{a\gamma} < 8.8 \cdot 10^{-11} GeV \text{ at } 95\% \text{ CL for } m_a \leq 0.02 eV.$$

Phase II-4He System started taking data in 2005. It was terminated in 2006 and resulted to a new limit to axion-to-photon coupling

$$g_{a\gamma} < 2.3 \cdot 10^{-10} GeV \text{ at } 95\% \text{ CL for } 0.02\ eV \leq m_a \leq 0.4\ eV.$$

Phase II-3He System started taking data in 2008. Till today it has searched in the mass region $0.39\ eV \leq m_a \leq 0.64\ eV$ and has given a new limit for the axion-to-photon coupling

$$g_{a\gamma} < 2.27 \cdot 10^{-11} GeV \text{ at } 95\% \text{ CL for } 0.02\ eV \leq m_a \leq 0.4\ eV.$$

CAST aims to continue axion searching to $m_a \leq 1.15\ eV$, this way overlapping with cosmological hot dark matter bounds.

ACKNOWLEDGEMENTS

First of all, I would really ike to thank Professor K. Zioutas for the hospitality in the CAST experiment and my colleagues in the CAST experiment for our smooth collaboration and the precious advice given.

Most of all my collaborators, I would like to thank Dr. T. Papaevangelou, who supervised every task I undertook for the whole period I occupied myself with the experiment. His contribution to my journey is of a great importance and irreplaceable.

Finally, nothing would have happened if it hadn't been for the help of Professor E. Gazis. From the very bottom of my heart I thank him for the opportunity to exist in the scientific environment of CERN, for his patience, the support and his trust.

BIBLIOGRAPHY

1. Abbon P. et al., The Micromegas Detector of the CAST Experiment, New Journal of Phys. 9 (2007) 170.
2. Arik M. et al., Search for Sub-eV Mass Solar Axions by the CERN Axion Solar Telescope with 3He Buffer Gas, Phys. Rev. Lett. 107 (2011) 261302
3. Bahcall J. N. and Pinsonneault M. H., What do we (not) know theoretically about solar neutrino fluxes?, Phys. Rev. Lett. 92 (2004) 121301.
4. Barr S. M., Solving the Strong CP Problem without the Peccei-Quinn Symmetry, Phys. Rev. Lett. 53 (1984) 329.
5. Barth K. et al., Commissioning and first operation of the cryogenics for the CERN Axion Solar Telescope (CAST), AIP Conference Proceeding 710 (2004) 168.
6. Van Bibber K. et al., Proposed experiment to produce and detect light pseudoscalars, Phys. Rev. Lett. 59 (1987) 759.
7. Van Bibber K., McIntyre P. M., Morris D. E., and Raffelt G. G., Design for a Practical Laboratory Detector for Solar Axions, Phys. Rev. D. 39 (1989) 2089.
8. Cantatore G. for the CAST Collaboration, Search for low Energy solar Axions with CAST, arXiv:0809.4581v2 (2009)
9. Charpak G. et al., Micromegas, A Multipurpose Gaseous Detector, Nucl. Instrum. Methods Phys. Res. A 478 (2002) 26-36.
10. Dafni T.,A Search for Solar Axions with the MICROMEGAS Detector in CAST, PhD Thesis, Technische Unversität Darmstadt (2005).
11. Dine M., TASI Lectures on the Strong CP Problem, hep-th/0011376 (2000).
12. Feng J. L., Dark Matter Candidates from Particle Physics and Methods of Detection, arXiv:1003.0904v2 (2010)
13. Ferrer-Ribas E. for the CAST Collaboration, Solar axion search with the CAST experiment, arXiv:0810.1874v1 (2008)
14. Ferrer-Ribas E. for the CAST Collaboration, The CAST Experiment: Status And Perspectives, arXiv:0912.4222v1 (2009)
15. Galán Lacarra J., Probing eV-mass scale Axions with a Micromegas Detector in the CAST Experiment, Universidad de Zaragoza (2012).
16. Giomataris Y. et al., Micromegas: A High-Granularity Position-sensitive Gaseous Detector for High Particle-Flux Environments, Nucl. Instrum. Methods Phys. Res. A 376 (1996) 29-35.
17. Griffiths D., Introduction to Elementary Particles , Wiley (1987).
18. Halzen F., Martin A. D., Quarks & Leptons: An Introductory Course in Modern Particle Physics, Wiley (1984).
19. Inoue K. & Yamatsu N., An approach to strong CP problem without axion, Institute for Cosmic Ray Research Theory Meeting (2008)
20. Kim J. E., Weak Interaction Singlet and CP Invariance, Phys. Rev. Lett. 43 (1979) 103.
21. Kim J. E., A Review on Axions and the Strong CP Problem, arXiv:0909.3908v1 (2009)
22. Kuster M. et al., The X-Ray Telescope of CAST, New Journal of Phys. 9 (2007) 169.

23. Moriyama S. et al., Direct Search for Solar Axions by Using Strong Magnetic Field and X-Ray Detectors, Phys. Lett. B 434 (1998) 147.
24. Nelson D. R., Partially Quenched Chiral Pertubation Theory and a Massless Up Quark: A Lattice Calculation of the Light-Quark-Mass Ratio, Dissertation, Graduate School of the Ohio State University (2002).
25. NOVAS (Naval Observatory Vector Astrometry Subroutines), http://aa.usno.navy.mil/software/
26. Peccei R. D. and Quinn H. R., CP Conservation In The Presence Of Pseudoparticles, Phys. Rev. Lett. 38 (1977) 1440.
27. Peccei R. D. and. Quinn H. R, Constraints imposed by CP conservation in the presence of pseudoparticles, Phys. Rev. D 16 (1977) 1791.
28. Weinberg S., The UA(1) Problem, Phys. Rev. D. 11 (1975) 3583.
29. Peccei R. D., CP-Violation Advanced Series in High Energy Physics, Vol 3 ed, C. Jarlskog, World Scientific (1989)
30. Peccei R. D., Particle Physics Footprints of the Invisible Axion, Physica Scripta T36 (1991)
31. Peccei R. D., The Strong CP Problem and Axions, arXiv:hep-ph/0607268v1 (2006)
32. Peccei R. D., Why PQ?, arXiv:1005.0643v1 (2010)
33. Universidad de Zaragoza (2008).
34. Perkins D., Particle Astrophysics, Oxford University Press (2003).
35. Primakoff H., Photo-Production of Neutral Mesons in Nuclear Electric Fields and the Mean Life of Neutral Meson, Phys. Rev. 81 (1951) 899.
36. Raffelt G. G., Stars as Laboratories for Fundamental Physics, University of Chicago Press (1996)
37. Raffelt G. G., Particle Physics from Stars, Annu. Rev. Nucl. Part. Sci. 49 (1999) 163-216
38. Raffelt G., Axions - Motivation, Limits and Searches, Presentation in Pont d'Avignon, Avignon (2008).
39. Rio Duarte Elias N. A. et al., Technical Design Report of the CAST 3He Gas System, CERN-SPSC-2006-029, (2006).
40. Ringwald A. et al., Proceedings of the 4th Patras Workshop on Axions, WIMPs and WISPs, DESY, Hamburg (2008)
41. Ruz J., Search for solar axions with the Time Projection Chamber of the CERN Axion Solar Telscope with 4-Helium as buffer gas, PhD Thesis, Universidad de Zaragoza (2009)
42. Sikivie P., Axion Searches, Nucl. Phys. Proc. Suppl. 87 (2000) 41
43. Sikivie P., Dark Matter Axions, arXiv:0909.0949v1 (2009)
44. Weinberg S., A New Light Boson?, Phys. Rev. Lett. 40 (1978) 223.
45. Wilczek F., Problem Of Strong P And T Invariance In The Presence Of Instantons, Phys. Rev. Lett. 40 (1978) 279
46. Vogel J. K., Searching for Solar Axions in the eV-Mass Region with the CCD Detector at CAST, PhD Thesis, Albert-Ludwigs-Universität Freiburg (2009)
47. Zioutas K. et al., First Results from the CERN Axion Solar Telescope (CAST), Phys. Rev. Lett. 94 (2005) 121301.
48. Zioutas K. et al., An improved limit on the axion-photon coupling from the CAST experiment, Journal of Cosm. and Astropart. Phys. 4 (2007) 010.

49. Zioutas K. et al. (CAST Collaboration), Probing eV-Scale Axions with CAST, Journal of Cosmology and Astroparticle Physics 02 (2009), 008.
50. Vogel J. K., Searching for Solar Axions in the eV-Mass Region with the CCD Detector at CAST, PhD Thesis, Albert-Ludwigs-Universität Freiburg (2009)